J. of Supercritical Fluids 57 (2011) 9–24

Contents lists available at ScienceDirect

The Journal of Supercritical Fluids

journal homepage: www.elsevier.com/locate/supflu

Computation of solid–fluid–fluid equilibria for binary asymmetric mixtures in wide ranges of conditions

S.B. Rodriguez-Reartes[a], M. Cismondi[b], M.S. Zabaloy[a,*]

[a] PLAPIQUI – Universidad Nacional del Sur, CONICET CC 717, 8000 Bahía Blanca, Argentina
[b] Facultad de Ciencias Exactas Físicas y Naturales, Universidad Nacional de Córdoba, Av. Vélez Sarsfield 1611, Ciudad Universitaria, X5016GCA, Córdoba, Argentina

ARTICLE INFO

Article history:
Received 6 July 2010
Received in revised form 2 February 2011
Accepted 8 February 2011

Keywords:
Solid–fluid–fluid equilibrium
Numerical continuation method
Binary systems
High pressure
Equation of state

ABSTRACT

In this work, we propose and test a numerical continuation method (NCM) for calculating solid–fluid–fluid (SFF) equilibrium loci for binary asymmetric systems. Such loci generally exist over a wide range of conditions. The method is able to track SFF lines of varying shape and degree of non-linearity. When building a curve for which, as in the case of a SFF curve, every point is defined by a non-linear system of equations, NCMs have the ability of selecting, among the variables involved, the optimum one, i.e., the variable that should be specified for calculating the next point on the curve. The initial guess for such next point is, when using NCMs, more sophisticated than simply setting it equal to the previously converged point of the curve. These features of NCMs make possible to track complete SFF lines with minimum user intervention. Among other algorithms, we propose in this work a procedure to obtain SFF lines that have been previously regarded as difficult to compute due to the very low concentration of the heavy component of the binary asymmetric system in either fluid phase. We illustrate the use of the present algorithms for a model that uses the Peng-Robinson equation of state (EOS) for the fluid phases, and an equation that relates the fugacity of the pure heavy component with pressure and temperature. We do not consider in this work the precipitation of the light component.

1. Introduction

The accurate description of the equilibria involving solid phases is a problem of great interest for industry [1]. In the petroleum and gas industry, the precipitation of paraffins, asphaltenes, gas hydrates and sulphur [2–4] has a great technological impact and can produce problems during extraction, transport and processing of petroleum. On the other hand, the increasing use of different techniques (rapid expansion of supercritical solution, RESS; gas anti-solvent process, GAS; supercritical anti-solvent process, SAS; solution enhanced dispersion by supercritical fluids, SEDS, etc.) for the formation of microparticles with special applications in pharmaceutical, nutraceutical, cosmetic and polymer industries [5,6] also requires a deep enough knowledge of the phase behavior involving solid phases.

A model for the solid–fluid equilibria of a multicomponent system should be able, as a necessary condition, to reproduce the experimental behavior of the binary sub-systems. The fluid phase equilibria of binary systems was characterized by van Konynenburg and Scott [7,8] who proposed a classification of the fluid phase behavior of such systems. This classification is based on the location of the critical loci and of the liquid–liquid–vapor (LLV) equilibrium lines in the pressure–temperature projection of the univariant lines of the binary system (PTUL diagram). The formation of pure solid phases in a binary system produce the interruption of LLV lines or of critical lines, in the PTUL diagrams of van Konynenburg and Scott [7], through the appearance of quadruple points (where four phases are at equilibrium) or of new critical end points (where a pure solid phase is at equilibrium with a critical fluid phase). From such special points, new three-phase equilibrium lines, involving at least a solid phase, arise. The resulting phase behavior is shown in the schematic pressure–temperature projections of Figs. 1–6, which correspond to types A to F in the classification of Yamamoto et al. [9], enhanced here by the incorporation of the low temperature region.

Figs. 1–6 show non-variant points and univariant lines that arise at conditions under which the components of the binary system can precipitate as pure solids. For instance, Fig. 4 presents, on one hand, conventional upper critical end points (UCEPs) and lower critical end points (LCEPs) where a critical phase is at equilibrium with a fluid phase. On the other hand, Fig. 4 shows a critical end point (3rd CEP) where a critical fluid phase is at equilibrium with a solid phase ($CEP_{cf\text{-}s}$). Three different types of $CEP_{cf\text{-}s}$s can be identified [9]. A First Critical End Point (1st CEP, Fig. 6) is the intersection point between a liquid–vapor critical line (L = G) stemming from the critical point of the more-volatile component, and a solid2–liquid–vapor (S_2LV) line (solid2 corresponds to a pure

* Corresponding author. Tel.: +54 291 486 1700x232; fax: +54 291 486 1600.
E-mail address: mzabaloy@plapiqui.edu.ar (M.S. Zabaloy).

0896-8446/$ – see front matter © 2011 Elsevier B.V. All rights reserved.
doi:10.1016/j.supflu.2011.02.004

Nomenclature

1	light compound
1st CEP	first critical end point
2	heavy compound
2nd CEP	second critical end point
3rd CEP	third critical end point
C1	critical point of the pure light compound (see Fig. 1)
C2	critical point of the pure heavy compound (see Fig. 1)
C_1, C_2, C_3	constants that characterize the melting curve of pure compound 2 (i.e., of the pure heavy component) (see Appendix B within the supplementary material)
E	equilibrium
$\hat{f}_i$	fugacity of component "i" in a fluid phase
f_2^S	fugacity of component 2 (i.e., of the heavy component) as a pure solid
HT	high temperature
L	liquid phase
LCEP	lower critical end point
LLV	liquid–liquid–vapor
LP	low pressure
LT	low temperature
LV	liquid–vapor
NCM	numerical continuation method
P	absolute pressure
P_{tp}	pure compound triple point (absolute) pressure
Q	quadruple point
R	universal gas constant
S	solid phase
SF	solid–fluid
SFF	solid–fluid–fluid
SL	solid–liquid
SLL	solid–liquid–liquid
SLV (Q-LT)	SLV line that originates at the Q point and extends indefinitely to low temperatures
SLV (Q-TP)	SLV line connecting the Q point and the triple point of the heavy compound
SLV (TP-LT)	SLV line that originates at the triple point of the heavy compound and extends indefinitely to low temperatures
SLV	solid–liquid–vapor
SLV-HT	SLV line from the triple point of the heavy compound to the 2nd CEP
SLV-LT	SLV line from 1st CEP to low temperature
S_{spec}	specification parameter
SV	solid–vapor
T	absolute temperature
TP	pure compound triple point
T_{tp}	pure compound triple point (absolute) temperature
UCEP	upper critical end point
V	vapor phase
υ_o	molar volume of the pure heavy component, in (subcooled) liquid state at system T and P.
$\Delta\upsilon^{S-L}$	solid–liquid molar volume difference for the pure heavy compound
υ_y and υ_x	molar volumes of the fluid phases at SFE conditions
x_1	mole fraction of component 1 (i.e., of the light component)
y_2	mole fraction of component 2 (i.e., of the heavy component)
Δh^f	enthalpy change on fusion

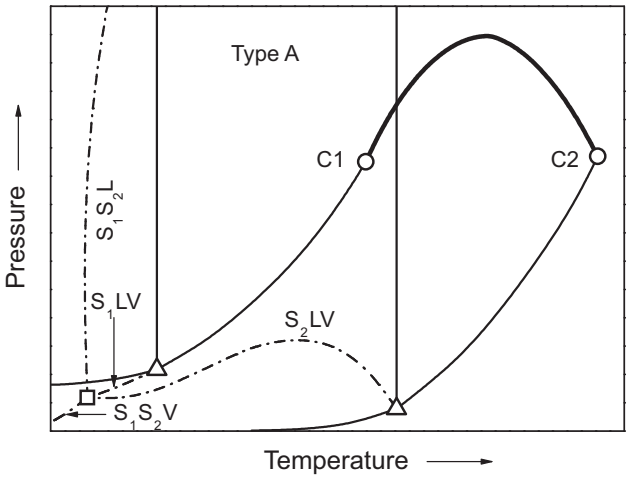

Fig. 1. Schematic pressure (P)–temperature (T) projection of univariant lines for TYPE A phase behavior for binary systems according to the classification of Yamamoto et al. [9]. (—) Critical locus, (—) pure compound saturation curve (vapor–liquid, solid–liquid or vapor–solid), (-.-.-.) three-phase curves: solid1–solid2–liquid (S_1S_2L), solid1–solid2–vapor (S_1S_2V), solid1–liquid–vapor (S_1LV), solid2–liquid–vapor (S_2LV), circle: pure compound critical point, empty triangle: pure compound triple point, □: quadruple point (Q).

heavy compound solid phase). 1st CEPs are observed in type F diagrams (Fig. 6). A Second Critical End Point (2nd CEP, Fig. 6) is the intersection point between a liquid–vapor critical line originated at the critical point of the less-volatile compound and a solid2–liquid–vapor curve stemming from the triple point of the same compound. 2nd CEPs are observed also in type F diagrams (Fig. 6). A 3rd CEP (e.g., Fig. 3) appears when a solid2–liquid–liquid line meets a liquid–liquid critical line (L = L). 3rd CEPs are observed in diagrams of type C, D and E (Figs. 3–5, respectively). In Figs. 1–6 we find two types of quadruple points (Q). In a SSLV Q point two solid phases (solid1, solid2), a liquid phase and a vapor phase coexist. SSLV Q points appear in the low temperature region for all types of solid–fluid behavior, i.e., from A (Fig. 1) to F (Fig. 6). In a SLLV Q point a solid phase (solid2), a vapor phase and two different liq-

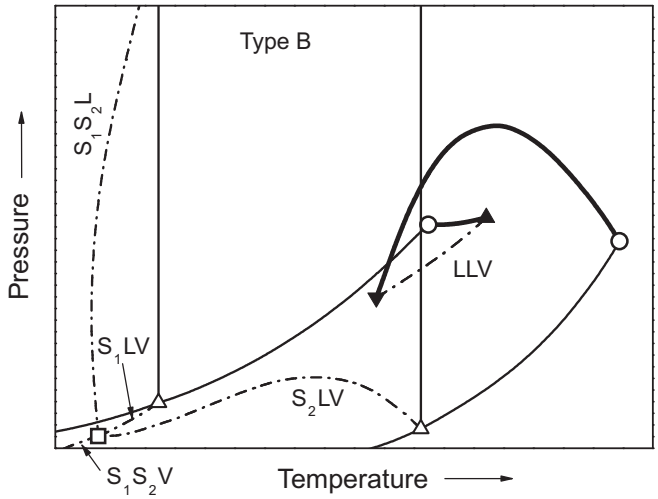

Fig. 2. Schematic PT projection of univariant lines for TYPE B phase behavior for binary systems according to the classification of Yamamoto et al. [9]. (—) Critical locus, (—) pure compound saturation curve (vapor–liquid, solid–liquid or vapor–solid), (-.-.-.) three-phase curves: liquid–liquid–vapor (LLV), solid1–solid2–liquid (S_1S_2L), solid1–solid2–vapor (S_1S_2V), solid1–liquid–vapor (S_1LV), solid2–liquid–vapor (S_2LV), circle: pure compound critical point, empty triangle: pure compound triple point, □: quadruple point (Q), ▲ UCEP, upside-down full triangle: LCEP.

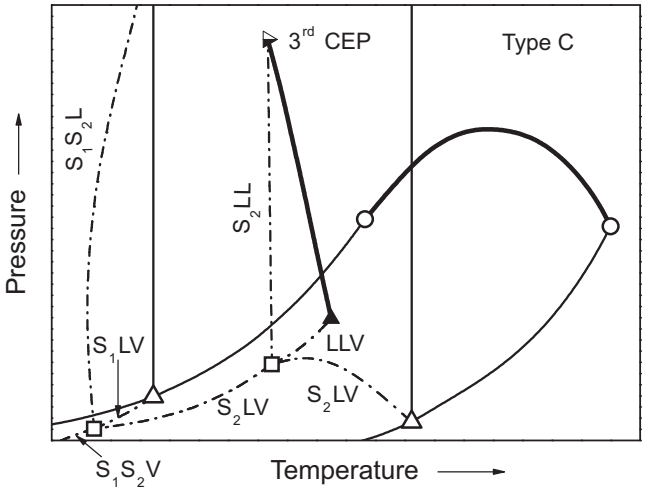

Fig. 3. Schematic *PT* projection of univariant lines for TYPE C phase behavior for binary systems according to the classification of Yamamoto et al. [9]. (—) Critical locus, (—) pure compound saturation curve (vapor–liquid, solid–liquid or vapor–solid), (-.-.-.) three-phase curves: liquid–liquid–vapor (LLV), solid1–solid2–liquid (S_1S_2L), solid1–solid2–vapor (S_1S_2V), solid1–liquid–vapor (S_1LV), solid2–liquid–vapor (S_2LV), solid2–liquid–liquid (S_2LL), circle: pure compound critical point, empty triangle: pure compound triple point, □: quadruple point (Q), ▲ UCEP, half-full triangle: 3rd CEP.

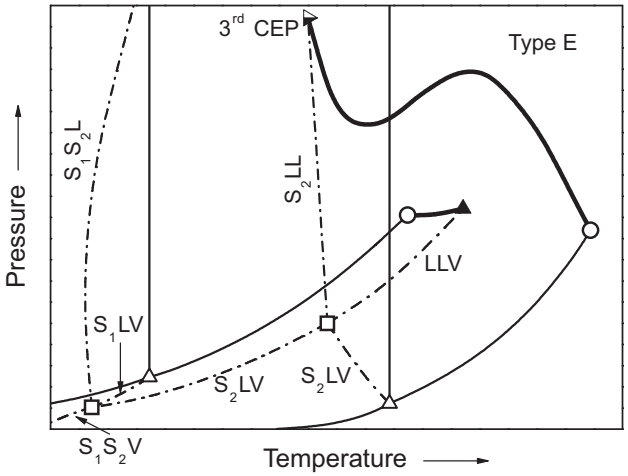

Fig. 5. Schematic *PT* projection of univariant lines for TYPE E phase behavior for binary systems according to the classification of Yamamoto et al. [9]. (—) Critical locus, (—) pure compound saturation curve (vapor–liquid, solid–liquid or vapor–solid), (-.-.-.) three-phase curves: liquid–liquid–vapor (LLV), solid1–solid2–liquid (S_1S_2L), solid1–solid2–vapor (S_1S_2V), solid1–liquid–vapor (S_1LV), solid2–liquid–vapor (S_2LV), solid2–liquid–liquid (S_2LL), circle: pure compound critical point, empty triangle: pure compound triple point, □: quadruple point (Q), ▲ UCEP, half-full triangle: 3rd CEP.

uids coexist. A SLLV Q point is characteristic of diagrams of type C, D and E (Figs. 3–5, respectively). From a given Q point, four three-phase equilibrium lines stem. All of them are schematically shown in Figs. 1–6. It is worth noting that all diagrams that we show in this work account for the recommended nomenclature for phase diagrams [10]. Since Ref [10] makes no suggestions for the $CEP_{cf\text{-}s}$ case, we adopted our own nomenclature.

The classification of Yamamoto et al. [9] seems quite comprehensive. Pressure–temperature projections of the type of Figs. 1–6 can also be found in references [8,9,11–14]. Garcia and Luks [12] have provided examples of real systems with behaviors corresponding to Figs. 1–6. It is interesting to point out that Labadie et al. [13] have obtained, for the case of a relatively simple thermodynamic model, patterns more complex than those of Figs. 1–6.

Much effort has been devoted to the experimental study of SFF equilibria [9,16–23]. Yamamoto et al. [9] have studied experimentally the binary systems formed by indole and different solvents, i.e., CO_2, C_2H_4, C_2H_6 and CHF_3. All these systems correspond to type F phase behavior (Fig. 6). Also, Yamamoto et al. [9] have studied the systems quinoxaline + C_2H_4 (type F, Fig. 6), quinoxaline + CHF_3 (type E, Fig. 5), quinoxaline + C_2H_6 (type E), and quinoxaline + CO_2 (type B or D, Figs. 2 and 4). Besides, Yamamoto et al. [16] studied several binary mixtures which display type A phase behavior (Fig. 1): pyrimidine + CO_2 and CHF_3; and pyrazine + CO_2 and CHF_3. Moreover, the mentioned authors [16], presented experimental data of three binary systems showing type E phase behavior: pyrimidine + C_2H_4 and C_2H_6, and pyrazine + C_2H_6; and

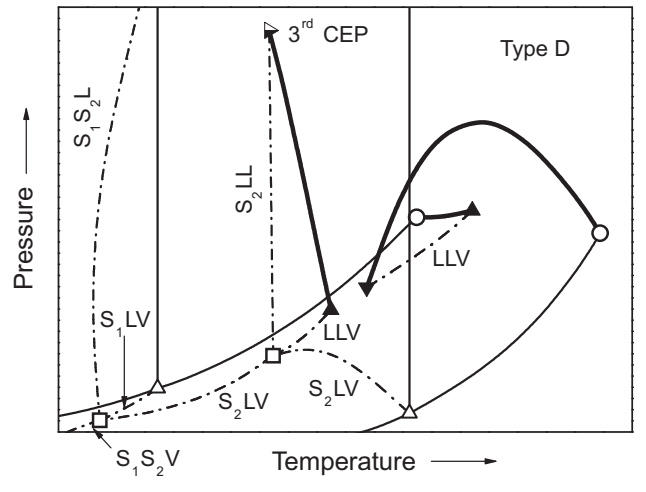

Fig. 4. Schematic *PT* projection of univariant lines for TYPE D phase behavior for binary systems according to the classification of Yamamoto et al. [9]. (—) Critical locus, (—) pure compound saturation curve (vapor–liquid, solid–liquid or vapor–solid), (-.-.-.) three-phase curves: liquid–liquid–vapor (LLV), solid1–solid2–liquid (S_1S_2L), solid1–solid2–vapor (S_1S_2V), solid1–liquid–vapor (S_1LV), solid2–liquid–vapor (S_2LV), solid2–liquid–liquid (S_2LL), circle: pure compound critical point, empty triangle: pure compound triple point, □: quadruple point (Q), ▲ UCEP, upside-down full triangle: LCEP, half-full triangle: 3rd CEP.

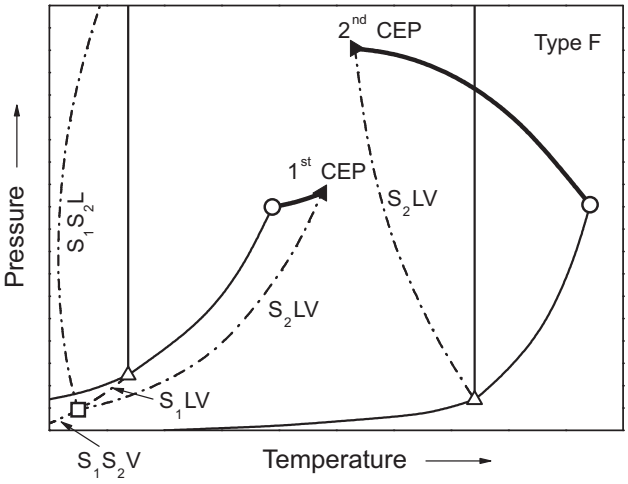

Fig. 6. Schematic *PT* projection of univariant lines for TYPE F phase behavior for binary systems according to the classification of Yamamoto et al. [9]. (—) Critical locus, (—) pure compound saturation curve (vapor–liquid, solid–liquid or vapor–solid), (-.-.-.) three-phase curves: solid1–solid2–liquid (S_1S_2L), solid1–solid2–vapor (S_1S_2V), solid1–liquid–vapor (S_1LV), solid2–liquid–vapor (S_2LV), circle: pure compound critical point, empty triangle: pure compound triple point, □: quadruple point (Q), ◄ 1st CEP, ▷ 2nd CEP.

they also showed an additional system displaying type F behavior, i.e., pyrazine + C_2H_4. Gregorowicz and co-workers [17] have presented SFF experimental data for the system n-eicosane + propane, which was identified to display type A behavior. The experimental data from Huie and co-workers [20] for the system n-eicosane + CO_2 correspond to type E behavior. The binary systems methane + n-eicosane [22], methane + n-tetracosane [18] and methane + n-triacontane [23] have been experimentally studied and it was determined that they present type F phase behavior (Fig. 6). Peters and co-workers [19,21] have reported experimental data for the binary systems ethane + pentacosane and ethane + tetracosane which display type E phase behavior (see Fig. 5). Although most of the authors of the works mentioned in this paragraph have presented schematic representations of the observed SFF behavior for the experimentally studied systems, no actual SFF physical-model-based equilibrium calculations under the conditions of the experimental data are available in such contributions. The absence of calculated SFF curves could be related, on one hand, to the difficulty of proposing a model with acceptable quantitative performance, and, on the other, to the complexity associated to the computation of SFF lines.

Binary Solid–fluid–fluid (SFF) equilibrium points are key points of binary isothermal or isobaric or isoplethic equilibrium diagrams [15]. Such diagrams are cuts of equilibrium surfaces existing in the pressure–temperature–composition space. Therefore, for obtaining such cuts, for a chosen model and chosen values for the model parameters, it is important to previously compute, among other important univariant lines, the (SFF) equilibrium lines. Due to the variety of shapes for the SFF lines that Figs. 1–6 show, the algorithms for calculating SFF lines should be robust.

From the phase rule, the number of degrees of freedom corresponding to a SFF equilibrium point equals unity for a binary system. The calculation of solid–fluid–fluid equilibrium lines has been carried out by some authors [12,13,24,25]. Garcia and Luks [12] have computed SFF equilibrium lines by solving the SFF isofugacity conditions at fixed values of temperature using a Newton-Raphson driven solution technique.

Labadie et al. [13] have added calculated critical lines to the diagrams of Ref. [12]. For the model system ethane + n-heptacosane, Garcia and Luks ([12], p. 99) have reported difficulties for computing a S_2LV line which corresponds to the one that connects the two quadruple points in Fig. 3, while, for the same model system, Labadie et al. ([13], p. 17) have shown a calculated segment of such S_2LV, but within a very narrow temperature range, of about 1 K.

Corazza et al. [24] have solved the SFF isofugacity conditions for building complete SLV equilibrium lines, limiting their calculations to the high temperature SFF branch of type F systems (S_2LV curve containing the 2nd CEP in Fig. 6).

Carter and Luks [25] present a SLV equilibrium curve obtained for a type A system. It seems that these authors have computed each SLV point by searching for the pressure value, at set temperature, at which the solid, liquid and vapor phases have a common plane, tangent to the surface of the Gibbs energy change on mixing. The authors seem to have done so by looking for intersection points between a solid–liquid (SL) line and solid–vapor (SV) line, both at set temperature.

In the works on calculation of SFF lines that we have quoted above, either the computations were limited to a single type of SFF line or/and every point of a given SFF line was always obtained specifying the temperature. This specification choice seems adequate for lines such as the S_2LV line of Fig. 5, which is not steep. It would not be so for the steep S_2LL line, also of Fig. 5. In this last case, specifying the value for pressure is clearly a better choice. SFF lines as the S_2LV line that ends at the 2nd CEP in Fig. 6, can have a temperature minimum [14]. This implies that specifying the temperature would not be adequate for temperatures close enough to the minimum temperature. Specifying the pressure for calculating a S_2LV line as that in Fig. 2 will not work in the vicinity of the point where the pressure presents a local maximum. It is possible to release the user from deciding which variable should be specified for computing a given SFF point, if the SFF equilibrium lines are built by applying a numerical continuation method (NCM). NCMs have the ability of selecting, among the variables involved in a given system of equations with one degree of freedom, the optimum one, i.e., the variable that should be specified for calculating the next point of the curve. In general, different points of a SFF line are obtained by specifying different variables in a NCM. NCMs are also named "curve tracking" methods, or "tracing" methods or "path following" methods [26]. Conventionally, when building a phase equilibrium line, after a converged point has been obtained, the initialization of the next point is performed by setting the initial guess equal to the last converged point. Otherwise, NCMs use a more elaborated approach, less prone to convergence failure. The features of NCMs make, in principle, possible to track complete SFF lines with minimum user intervention, e.g., the user does not need to wonder whether the SFF lines to be computed are or not highly non-linear in order to decide how to conduct the calculations. NCMs should be able to track SFF lines of varying shapes, as, e.g., those shown in Figs. 1–6, without failing to converge in the vicinity of local minima or maxima.

Michelsen [27] and Michelsen and Mollerup [28] described the use of NCMs for calculating multicomponent phase envelopes using equations of state (EOS). More recently, NCMs have been described and used for generating binary critical lines, liquid–liquid–vapor lines and azeotropic lines ([15,29,30]), and also Pxy and Txy diagrams [31]. References [15,29–31] considered equilibria not involving solid phases. In this work, we propose, describe and test a NCM for calculating solid–fluid–fluid equilibrium loci, of varying shape and degree of non-linearity, for binary asymmetric systems, over wide ranges of conditions. This NCM makes possible to track complete SFF lines with minimum user intervention. Among other algorithms, we propose a special procedure to obtain SFF lines that have been previously regarded as difficult to compute ([12], p. 99), due to the very low concentration of the heavy component of the binary asymmetric system in either fluid phase. We illustrate the use of the present algorithms for a model that uses the Peng-Robinson equation of state for the fluid phases, and an equation that makes possible to compute the fugacity of the pure heavy component at given pressure and temperature. The model assumes that the solid phase is formed by the pure heavy compound [32], i.e., we account in this work neither for the precipitation of solid solutions nor for the precipitation of the light component of the binary system. This is a good approximation, at high enough temperature, for asymmetric mixtures, i.e., for mixtures made of compounds with significant differences in their chemical nature or in their molecular mass. We also report in this work how we calculate binary quadruple equilibrium points and critical end points where a critical fluid phase is at equilibrium with a solid phase. Additionally, we describe a parameterization technique that makes possible to fit solid–fluid equilibrium experimental data for mixtures while leaving invariant, during the optimization process, the description of the fluid phases and of the solid–liquid equilibrium curves of the pure substances (Appendix B within the supplementary material).

The scope of this work is to provide a robust tool, that improves on previous calculation practice, for the generation of complete binary SFF equilibrium lines, when a choice of a model and of values for the model parameters has been made, i.e., our attention is not focused here on the extent to which such calculated SFF lines quantitatively compare with experimental data, but on the robust computation of SFF lines having shapes as varied as those that have been observed in the laboratory (Figs. 1–6). As an application example, we use our proposed NCMs to characterize the behavior of the system CO_2 + Progesterone from the limited isoplethic fluid–fluid

and solid–fluid experimental equilibrium data recently obtained by Favareto et al. [33].

2. Thermodynamic model

To describe the fluid state of a binary mixture of a light component (labeled "1") and a heavy component (labeled "2"), we use a pressure-explicit equation of state, i.e., a relationship between the absolute pressure (P), the absolute temperature (T), the mixture molar volume (υ) and the mixture composition z_2, where z_2 is the mole fraction of component "2". We represent such relationship as $P = h_{PVT}(T, z_2, \upsilon)$, where the form of function h_{PVT} corresponds to the adopted EOS, e.g., to the Peng-Robinson (PR) [34] EOS, i.e., the EOS that we used in this work. The h_{PVT} function, imposes the expression for the fugacity of component "i" in the fluid mixture ($\hat{f}_i$). Thus, $\hat{f}_i$ depends on the same variables than function h_{PVT}, i.e., $\hat{f}_i = \hat{f}_i(T, z_2, \upsilon)$. Indeed, this last functional relationship also corresponds in this work to the PR-EOS.

Due to the high asymmetry of the binary systems that we consider in this work, we assume that a given solid phase is made of only the pure heavy component (component "2"). Thus, for performing equilibrium calculations, we need an equation relating the fugacity of the pure component "2" in solid state to the absolute pressure (P) and to the absolute temperature (T) of the system. Following Refs. [32,35] (see Appendix B in the supplementary material), we define, mathematically, the fugacity of the pure heavy component "2" in solid state at T and P, i.e., $f_2^S(T, P, \upsilon_o)$, (where υ_o actually depends on T and P) as follows:

$$f_2^S(T, P, \upsilon_o) = \hat{f}_2(T, 1, \upsilon_o)\exp(U) \tag{1}$$

In Eq. (1), υ_o is the molar volume of the pure heavy component (component "2"), in (subcooled hypothetical) liquid state, at T and P. Such pure liquid has a fugacity $\hat{f}_2(T, 1, \upsilon_o)$ [first factor within the right hand side of Eq. (1)]. Notice that expression $\hat{f}_2(T, 1, \upsilon_o)$ simply states that the function $\hat{f}_i = \hat{f}_i(T, z_2, \upsilon)$, with subscript "i" set equal to "2", is evaluated at $z_2 = 1$ and at $\upsilon = \upsilon_o$, i.e., that the computed fugacity corresponds to a liquid made of the pure heavy compound, having such pure liquid a molar volume equal to υ_o. Both, υ_o and $\hat{f}_2(T, 1, \upsilon_o)$ are given in this work by the PR-EOS. The exponential factor in Eq. (1) relates [through Eq. (1)] the liquid state with the solid state for a pure substance at given temperature and pressure. The variable U, which depends on T and P, is defined as follows:

$$U = \frac{\Delta\upsilon^{S-L}}{RT_{tp}}\left[C_1\left(1 - \frac{T_{tp}}{T}\right) + C_2\left(\frac{T_{tp}}{T} - 1 + \ln\left(\frac{T}{T_{tp}}\right)\right) + C_3\left(\frac{T}{2T_{tp}} - 1 + \frac{T_{tp}}{2T}\right) + \frac{T_{tp}}{T}(P - P_{tp})\right] \tag{2}$$

In Eq. (2), the constants T_{tp}, P_{tp} (see Table 2), $\Delta\upsilon^{S-L}$, C_1, C_2 and C_3 correspond to the pure heavy component (component "2"). $\Delta\upsilon^{S-L}$ is the solid–liquid molar volume difference ($\upsilon_{solid} - \upsilon_{liquid}$). The constants C_1, C_2 and C_3 characterize the pure heavy component solid–liquid equilibrium curve (melting curve). R is the universal gas constant. We developed Eq. (1) from clear assumptions about the temperature dependency of the solid–liquid heat capacity difference (see Appendix B in the supplementary material).

To fix ideas, for computing $f_2^S(T, P, \upsilon_o)$ at set T and P, we would first calculate υ_o from the adopted EOS [$P - h_{PVT}(T, 1, \upsilon_o) = 0$], next we would compute $\hat{f}_2(T, 1, \upsilon_o)$, then U from Eq. (2), and, finally, plug the results into de right hand side of Eq. (1), to obtain the value of $f_2^S(T, P, \upsilon_o)$. We stress that the phase type for $f_2^S(T, P, \upsilon_o)$ is "solid" while the phase type for $\hat{f}_2(T, 1, \upsilon_o)$ is "liquid", and that both fugacities correspond to the same T and P values.

Notice that the pure liquid having a molar volume υ_o it is not, in general, at equilibrium with the pure solid. Otherwise, the fugacity of such pure liquid at T and P, i.e., $\hat{f}_2(T, 1, \upsilon_o)$, is a reference fugacity that has to be affected by the exponential factor in Eq. (1) so that the fugacity of the pure heavy component "2" in solid state at T and P can be computed. Only when the exponential factor in Eq. (1) equals unity, we have the pure solid at equilibrium with the pure liquid at T and P. In such a case, T and P are the coordinates of a point of the pure heavy compound solid–liquid equilibrium (melting) line.

The variable υ_o, i.e., a property of a pure liquid, appears as an argument for the fugacity of the pure solid [on the left hand side of Eq. (1)] because the fugacity of the pure solid is partially computed from the fugacity of the pure liquid, i.e., from a liquid-state reference fugacity, being the temperature and pressure for such reference fugacity the same than the temperature and pressure of the solid. We stress that the difference between the reference fugacity [$\hat{f}_2(T, 1, \upsilon_o)$] and the fugacity of interest [$f_2^S(T, P, \upsilon_o)$] does not lie on the pressure, temperature or composition conditions, but on the state of the pure substance, i.e., the liquid state corresponds to $\hat{f}_2(T, 1, \upsilon_o)$ and the solid state corresponds to $f_2^S(T, P, \upsilon_o)$. In summary, while the left hand side of Eq. (1), i.e., $f_2^S(T, P, \upsilon_o)$, represents only the pure solid, such pure solid fugacity depends on properties of a pure hypothetical liquid. This is a well established approach (see Appendix B in the supplementary material). An alternative approach would be to use an equation of state applicable only to the pure solid. In such an approach, the fugacity of the pure solid would only depend on temperature, on the molar volume of the solid and on parameters characteristic of the pure compound in solid state.

3. Calculation algorithms for solid–fluid–fluid equilibrium lines

As previously stated, we have only considered the possibility of precipitation of the pure heavy compound. We calculate solid–fluid–fluid (SFF) equilibrium lines using a numerical continuation method similar in its basic nature to the one that Michelsen [27] proposed for tracking phase envelopes in multicomponent mixtures.

The construction of a SFF equilibrium curve starts at a point known to belong to the SFF curve, i.e., at a S_2LLV quadruple point (Q), or at a point very close to the triple point (TP) of the pure heavy compound, or at a low temperature–low pressure SFF point (LTLP), in such order of preference. The TP has to be known, and the Q point computed, before starting the construction of the SFF lines of the binary system. A Q point might not exist (within the universe of the model), and such lack of existence should also be known before calculating the SFF lines. It is always possible, in principle, to compute a LTLP SFF point but often not necessary. Notice that a known point used to start the construction of a SFF line is a known solution of the system of Eqs. (3)–(9), described below. Subsequent points are calculated automatically through the continuation method, and the complete SFF equilibrium curve is traced out.

The system of equations to be solved for computing a SFF equilibrium point, for a binary system, where the solid phase is formed by the pure heavy component, is the following:

$$\ln(P) - \ln[h_{PVT}(T, 1, \upsilon_o)] = 0 \tag{3}$$

$$\ln(P) - \ln[h_{PVT}(T, 1 - x_1, \upsilon_x)] = 0 \tag{4}$$

$$\ln(P) - \ln[h_{PVT}(T, y_2, \upsilon_y)] = 0 \tag{5}$$

$$\ln[\hat{f}_1(T, 1 - x_1, \upsilon_x)] - \ln[\hat{f}_1(T, y_2, \upsilon_y)] = 0 \tag{6}$$

$$\ln[\hat{f}_2(T, 1 - x_1, \upsilon_x)] - \ln[\hat{f}_2(T, y_2, \upsilon_y)] = 0 \tag{7}$$

$$\ln[\hat{f}_2^S(T, P, \upsilon_o)] - \ln[\hat{f}_2(T, y_2, \upsilon_y)] = 0 \tag{8}$$

$$g_{spec}(T, P, x_1, y_2, \upsilon_x, \upsilon_y, \upsilon_o) - S_{spec} = 0 \tag{9}$$

Table 1
Specification functions used in this work for the calculation of solid–fluid–fluid equilibrium lines.

Identification number (NS)	Specification function $g_{spec}(T, P, x_1, y_2, \upsilon_x, \upsilon_y, \upsilon_o)$
1	$\ln(T)$
2	$\ln(P)$
3	$\ln(x_1)$
4	$\ln(y_2)$
5	$\ln(\upsilon_x)$
6	$\ln(\upsilon_y)$
7	$\ln(\upsilon_o)$

where T and P are the system temperature and pressure, x_1 is the mole fraction of the light component ("1") in one of the fluid phases (phase "x"), y_2 is the mole fraction of the heavy component ("2") in the other fluid phase (phase "y"), υ_x is the molar volume of phase "x" and υ_y is the molar volume of the phase "y". Notice that $f_2^S(T, P, \upsilon_o)$, i.e., the fugacity of the pure heavy component in solid state at system T and P, is defined by Eq. (1).

Eq. (3) establishes that the molar volume υ_o of the pure hypothetic liquid is set by the system temperature and pressure through the adopted EOS (which is defined by the function h_{PVT}). Similarly, Eqs. (4) and (5) imply that the same adopted EOS imposes how the system temperature and pressure relate to the composition (x_1) and molar volume (υ_x) of phase "x" [Eq. (4)] and to the composition (y_2) and molar volume (υ_y) of phase "y" [Eq. (5)]. The isofugacity (phase equilibrium) condition for component 1 (light component) in the fluid phases, is imposed by Eq. (6), while Eqs. (7) and (8) account for the isofugacity of component 2 (heavy component) in the fluid and solid phases.

The left hand sides of Eqs. (3)–(9) are the elements of a vector function F (e.g., $F(3) = \ln(P) - \ln[h_{PVT}(T, y_2, \upsilon_y)]$). The system of Eqs. (3)–(9), i.e., system $F = 0$, considers that the pressure P and temperature T are uniform throughout the three-phase system. The variables of system $F = 0$ are the elements of vector X, which is defined as follows:

$$X^T = [\ln(T), \ln(P), \ln(x_1), \ln(y_2), \ln(\upsilon_x), \ln(\upsilon_y), \ln(\upsilon_o)] \tag{10}$$

The logarithms in the above equation imply a proper scaling of the system variables.

Eq. (9) [$F(7) = 0$] is the "specification equation". We use it to make the number of unknowns become equal to the number of equations. $g_{spec}(T, P, x_1, y_2, \upsilon_x, \upsilon_y, \upsilon_o)$ is the "specification function", and S_{spec} is the "specification parameter". For instance, when computing a SFF equilibrium at 700 bar, we would set $g_{spec}(T, P, x_1, y_2, \upsilon_x, \upsilon_y, \upsilon_o) = \ln(P)$ and $S_{spec} = \ln(700)$. Eq. (9) thus implies, in this case, that $\ln(P) = \ln(700)$. In other words, when defining the g_{spec} expression together with the S_{spec} value we spend the single degree of freedom available for calculating a SFF equilibrium point of a binary system. Table 1 presents all the possible expressions for g_{spec} that we have used in this work.

After defining g_{spec} and S_{spec}, the full multidimensional Newton's method is used for solving the set of Eqs. (3)–(9). Thus, the X vector is updated, in a given iteration, by solving the following linear system of equations:

$$J \begin{pmatrix} \Delta \ln(T) \\ \Delta \ln(P) \\ \Delta \ln(x_1) \\ \Delta \ln(y_2) \\ \Delta \ln(\upsilon_x) \\ \Delta \ln(\upsilon_y) \\ \Delta \ln(\upsilon_o) \end{pmatrix} + F = 0 \tag{11}$$

where J is the Jacobian matrix corresponding to the vector function F.

The evaluation of J requires computing the partial derivatives of the elements of the vector function F with respect to all variables of vector X. Such derivatives are obtained analytically in this work. After convergence is reached, we compute the sensitivity vector dX/dS_{spec}, which is defined as follows:

$$\left[\frac{dX}{dS_{spec}}\right]^T = \left[\frac{d\ \ln(T)}{dS_{spec}}, \frac{d\ \ln(P)}{dS_{spec}}, \frac{d\ \ln(x_1)}{dS_{spec}}, \frac{d\ \ln(y_2)}{dS_{spec}}, \frac{d\ \ln(\upsilon_x)}{dS_{spec}}, \frac{d\ \ln(\upsilon_y)}{dS_{spec}}, \frac{d\ \ln(\upsilon_o)}{dS_{spec}}\right] \tag{12}$$

The sensitivity vector dX/dS_{spec} provides information on how the solution of the system of Eqs. (3)–(9) changes if we change the value of the specification parameter S_{spec}. This vector is calculated in a straightforward way, analogous to the one indicated in references [15,30,31], i.e., by solving the following linear system of equations:

$$J\left(\frac{dX}{dS_{Spec}}\right) + \left(\frac{\partial F}{\partial S_{Spec}}\right) = 0 \tag{13}$$

In Eq. (13), J is the Jacobian matrix evaluated at the converged solution of the system of Eqs. (3)–(9). Eq. (13) is easily obtained from deriving both sides of the system $F = 0$ with respect to S_{spec}, using the chain rule. Vector $\partial F/\partial S_{Spec}$ in Eq. (13) has all its components equal to zero, except for the last one, which equals minus one [$\partial F(7)/\partial S_{spec} = (-1)$], since $F(7)$ is the only component of F that depends explicitly on S_{spec}.

Once the first point of a SFF equilibrium line has been computed, i.e., after achieving convergence for the first time for the system of Eqs. (3)–(9), we proceed to calculate the next point of the SFF line. For that, we use the information that the sensitivity vector dX/dS_{spec} [obtained from Eq. (13)] provides. Vector dX/dS_{spec} makes possible to identify the best choice, among those of Table 1, for the expression of the specification function $g_{spec}(T, P, x_1, y_2, \upsilon_x, \upsilon_y, \upsilon_o)$, for computing the next point. The optimum expression is the one corresponding to the element of dX/dS_{spec} with largest absolute value. For instance, if the component of dX/dS_{spec} with largest absolute value is the third one [see Eq. (12)], then, we set $g_{spec}(T, P, x_1, y_2, \upsilon_x, \upsilon_y, \upsilon_o) = \ln(x_1)$. In this way, we identify among the variables of the system of Eqs. (3)–(9), the optimum one, i.e., the variable whose value should be specified to maximize the probability of achieving convergence when intending to calculate the next point of the SFF line. The initial estimate for the solution vector for such next point is obtained also taking advantage from the information contained in vector dX/dS_{spec} [15,30,31] as follows:

$$X^0_{\text{next point}} = X_{\text{converged point}} + \left[\frac{dX}{dS_{spec}}\right]_{\text{converged point}} \Delta S_{spec} \tag{14}$$

where superscript "0" means "initial estimate", while the user-imposed step length ΔS_{spec} is defined as follows:

$$\Delta S_{spec} = S_{\text{next point}} - S_{\text{converged point}} \tag{15}$$

Once we set a value for ΔS_{spec}, then, the value of $S_{\text{next point}}$ becomes imposed by Eq. (15), i.e., the single degree of freedom available for binary SFF equilibrium points becomes defined and it is possible to proceed to the calculation of the next SFF point. Notice that Eq. (14) assumes a linear behavior for the SFF line. From elementary calculus, this is always a good assumption as long as the range of conditions within which such assumption is adopted is sufficiently narrow. Thus, Eq. (14) will lead to convergence, when solving the system of Eqs. (3)–(9), only if ΔS_{spec} is set to have a small enough absolute value. The initialization scheme of Eq. (14) is more sophisticated and less prone to divergence than simply setting, as often done, the initial guess, for the next point of the SFF curve, as equal to the converged point, i.e., $X^0_{\text{next point}} = X_{\text{converged point}}$. The use

of the sensitivity vector to properly define the degree of freedom for the next point of a curve to be computed, and to initialize the variables of such point, is the distinguishing feature of the so-called numerical continuation methods.

The present algorithm allows any of the elements of vector X to be the specified variable, according to Table 1, in the computation of a SFF point. This flexibility partially contributes to minimizing the need for user intervention when computing a SFF line.

For calculating a new SFF point, we set the value of ΔS_{spec} considering the number of iterations (NIT) required to obtain the last converged point. If NIT ≤ 4, then, the absolute value of ΔS_{spec} is increased and, if NIT ≥ 6, it is decreased. If NIT = 5, then ΔS_{spec} remains unchanged. These criteria are overridden by an empirical limit set, for every variable of vector X, on the maximum absolute value of ΔS_{spec}. If convergence is not achieved within a pre-set maximum number of iterations when intending to solve the system $F = 0$, then, the algorithm automatically goes back to the previous point ($X_{\text{converged point}}$) and decreases the absolute value of ΔS_{spec}, i.e., of the step length, by a factor of two and computes a new initial estimate through Eq. (14).

The present algorithm is a numerical continuation method, and, as such, it should be able to track different types of SFF equilibrium curves, as those that Figs. 1–6 show.

In sections 3.1 to 3.4 we describe how we calculate special points of the SFF equilibrium lines.

3.1. Calculation of the S_2LLV quadruple point

In this work, we calculate binary Q points where three fluid phases and a single solid phase coexist, being such solid phase made of only the pure heavy compound (S_2). To compute a Q point, we first obtain the liquid–liquid–vapor equilibrium line as it was previously described [30]. Next, we search, along the calculated LLV line, for a LLV point for which the (fluid) fugacity of component "2" in the binary system (at LLV conditions) equals, within a preset tolerance, the fugacity of the pure compound "2" in solid state (at the LLV temperature and pressure). This last fugacity is calculated as described in the "Thermodynamic model" section. The result of this process is the computed coordinates of the Q point, i.e., the temperature, the pressure, the composition of the three fluid phases and the molar volumes of such phases. A converged quadruple point provides three converged SFF equilibrium points, one for each of the three SFF lines that originate at the Q point. Each of such converged points is a solution for the system of Eqs. (3)–(9).

3.2. Calculation of the heavy component triple point (TP)

The only experimental information we use for the TP is the TP temperature (T_{tp}). For consistency, we set the TP pressure P_{tp} as equal to the pure compound vapor–liquid equilibrium pressure, at the experimental triple point temperature T_{tp}, calculated using the pressure-explicit EOS adopted for representing the fluid state, i.e., the PR-EOS in this work. Such calculation also provides the computed values for the molar volumes of the fluid phases at the TP. From a practical standpoint, the computed TP of the pure heavy component ("2") is not a known point of the SFF line that originates at such TP (i.e., a known solution of the system $F = 0$). The reason is that at zero mole fraction for the light component ("1") the fugacity $\hat{f}_1$ in either fluid phase is zero and, therefore, Eq. (6), as it is written, is not directly applicable.

3.3. Calculation of a low temperature–low pressure (LTLP) SFF point

We start by calculating, at a quite low specified temperature, the vapor–liquid equilibrium point for the pure light compound ("1"), using the adopted EOS. Next, from computing the fugacity coefficients at infinity dilution of the heavy component ("2") in the pure component "1" as saturated vapor and liquid, we calculate a hypothetical solubility of component "2" in component "1" as a saturated vapor, and a hypothetical solubility of component "2" in component "1" as a saturated liquid. Next, we select one of the two previously calculated solubilities and estimate the fluid phase compositions at SFF equilibrium at the specified temperature. This process provides excellent initial values for the variables of vector X, which we use to compute the SFF point at the specified temperature. This procedure is based on assuming that the concentration of component "2" is very low in either fluid phase, at low enough temperature, under conditions of SFF equilibrium. Such assumption is a very good one for asymmetric systems. Appendix A provides the detailed steps to follow for computing a *LTLP SFF* point. Such point is useful to start building a complete SFF line.

At this point it is worth to note that for some cases it could be necessary to rewrite the set of equations $F = 0$ [Eqs. (3)–(9)] in terms of the variable x_2 instead of the variable x_1. This modification is necessary for highly asymmetric systems, for which the liquid phase at SFF conditions may have just some traces of the heavy component. In such a case, the x_1 value is very close to unity, and the logarithmic scaling of variable x_1 fails, due to round-off errors.

3.4. Calculation of critical end points

Although in this work we do not start the computation of SFF lines at CEPs (where a critical fluid phase is at equilibrium with a solid phase, i.e., $\text{CEP}_{\text{cf-s}}$), we do calculate them anyway to complete the characterization of the model + parameters behavior. To compute a 1st or a 2nd or a 3rd CEP we first calculate the critical lines of the system as previously described [30]. Next, we search, along a given critical line, for a point for which the (fluid) fugacity of component "2" in the binary critical phase equals, within a preset tolerance, the fugacity of the pure compound "2" in solid state (at the critical temperature and pressure). Notice that this procedure is analogous to the one described previously for calculating quadruple points.

In the next section we describe in detail the procedures for calculating different types of SFF equilibrium lines.

3.5. Calculation of solid–fluid–fluid equilibrium lines

As previously stated, first we obtain a solution of the system of Eqs. (3)–(9), and next we build the SFF line applying the NCM already described. The choice of the starting point for the construction of a SFF line depends on the nature of the starting point and of the end point of the SFF curve to be traced out. We developed procedures for calculating the following types of SFF lines:

I. SLV equilibrium curves which start at the Triple Point of the heavy component (TP) and end at a Second Critical End Point (2nd CEP, see Fig. 6):

   At the TP, the composition of the solid, vapor and liquid phases is the same, i.e., the mole fraction for the heavy component equals unity in any phase. We obtain a point, on the SFF line, located very close to the TP, as follows:

   - Set $x_1 = 2.5 \times 10^{-10}$.
   - Use $y_2 = [1 - 2.5 \times 10^{-10}]$ as initial estimate for y_2.
   - Use the T_{tp} as the initial estimate for T, and $P_{tp} + 0.0001$ as initial estimate for P.
   - Solve the *PVTx* relationship to generate initial estimates for υ_x, υ_y and υ_o.

   $$P = h_{PVT}(T, 1 - x_1, \upsilon_x);\ P = h_{PVT}(T, y_2, \upsilon_y);\ P = h_{PVT}(T, 1, \upsilon_o)$$

- Set $g_{spec}(T, P, x_1, y_2, \upsilon_x, \upsilon_y, \upsilon_o) = \ln(x_1)$ as the specification function and set $S_{spec} = \ln(2.5 \times 10^{-10})$, and solve the system of Eqs. (3)–(9).

Notice that we obtain a point, on the SFF line, located very close to the TP by setting x_1 equal to 2.5×10^{-10}. This value is relatively arbitrary and may be replaced by any other value (say 1.0×10^{-10}) provided that it is low enough. The reader should bear in mind that in our actual calculations the mole fraction is logarithmically scaled.

Choosing, as a starting point, a SFF point located very close to the TP is better than choosing the 2nd CEP: the 2nd CEP is actually a fluid–solid equilibrium point rather than a solid–fluid–fluid equilibrium point.

II. SLV equilibrium curves which start at the Triple Point of the heavy component (TP) and extend indefinitely towards low temperatures:

The lack of a low temperature end point is due to not having accounted for the precipitation of the light component in this work. Thus, the computed curve will not end at a S_1S_2LV quadruple point (see Figs. 1 and 2). A point of the SLV curve, located very close to the TP, is computed in the same way as described in item "I". In this case we stop the calculation of the SFF line at some Low Pressure–Low Temperature point. A point of the SLV curve, located very close to the TP, is the chosen starting point here because it has quite defined temperature, pressure and density conditions.

III. SLV equilibrium curves which begin at the First Critical End Point (1st CEP) and extend indefinitely towards low temperatures (see comments in item "II", and see Fig. 6):

The first converged point where we start building the SLV curve is a Low Pressure–Low Temperature (LPLT) point, which we obtain as described Appendix A. The first point of the SLV curve, i.e., the LPLT SLV point, is more difficult to obtain (Appendix A) than all the other points belonging to the SLV curve. The 2nd point is more easy to obtain than the first one thanks to the availability of the sensitivity vector computed from the information corresponding to the converged 1st point (LPLT point). Such vector makes possible to identify the optimum variable to be specified to carry out the computation of the 2nd point, and also to properly predict the solution vector for such 2nd point, according to Eq. (14). Similarly, the sensitivity vector calculated from the converged 2nd point facilitates the computation of the 3rd point of the SLV curve, an so on. The choice of the starting point in this case is justified on the fact that the 1st CEP is not (strictly) a three-phase equilibrium point.

IV. SLV equilibrium curves that start at a SLLV Q point and end at the TP of the pure heavy compound (see Figs. 3–5):

Once the Q point has already been obtained as explained in section 3.1, we follow the next steps:

- Set $T = TQ$, where TQ is the quadruple point temperature in K.
- Set $P = PQ$, where PQ is the quadruple point pressure in bar.
- Let x_1 and υ_x to be equal, respectively, to the composition and the molar volume of the liquid phase richer in the heavy compound at the Q point.
- Let y_2 and υ_y to be equal, respectively, to the composition and the molar volume of the vapor phase at the Q point.
- Let υ_o to be equal to the liquid molar volume of the pure heavy compound at TQ and PQ obtained with the adopted $PVTx$ relationship at the time of computing the Q point.
- Use $g_{spec}(T, P, x_1, y_2, \upsilon_x, \upsilon_y, \upsilon_o) = \ln(T)$ as the specification function and $S_{spec} = \ln(TQ)$ as the value for the specification parameter.

With the previous selected Q-point information, which corresponds to a known solution of system $F = 0$ [Eqs. (3)–(9)], we calculate the Jacobian matrix and then the sensitivity vector dX/dS_{spec} from Eq. (13). Next we identify the optimum variable to be specified, set a value for it, initialize the variables of vector X through Eq. (14), and proceed to obtain a SFF equilibrium point located on the SLV line very close to the Q point. The choice of the Q point as the starting point is justified on the fact that part of the information contained in the calculated (four-phase) Q point already constitutes a point of the (three-phase) SFF line to be built.

V. SLV equilibrium curves that start at a SLLV Q point and extend indefinitely to low temperatures (see Figs. 3–5):

The first converged point for curves of this kind is obtained in a way analogous to that described in item "IV". The difference is that here x_1 and υ_x are set equal, respectively, to the composition and the molar volume of the liquid phase richer in the light component under the Q point conditions. From the values of T, P, x_1, y_2, υ_x, υ_y and υ_o (known from the previously computed Q point), we calculate the sensitivity vector dX/dS_{spec} from Eq. (13) and proceed as in item "IV".

VI. SLL equilibrium curves that start at a SLLV Q point and end at a Third Critical End Point (3rd CEP) at high pressure (see Figs. 3 and 4):

Once the Q point has already been obtained we follow the next steps:

- Set $T = TQ$, where TQ is the quadruple point temperature in K.
- Set $P = PQ$, where PQ is the quadruple point pressure in bar.
- Let x and υ_x to be equal, respectively, to the composition and the molar volume of the liquid phase richer in the heavy compound at the Q point.
- Let y and υ_y to be equal, respectively, to the composition and the molar volume of the liquid phase richer in the light compound at the Q point.
- Let υ_o to be equal to the liquid molar volume of the pure heavy compound at TQ and PQ obtained with the $PVTx$ relationship at the time of computing the Q point.
- Use $g_{spec}(T, P, x_1, y_2, \upsilon_x, \upsilon_y, \upsilon_o) = \ln(T)$ as the specification function and $S_{spec} = \ln(TQ)$ as the value for the specification parameter, and proceed as in item "IV".

Summarizing, the general procedure for calculating an entire SFF line is as follows: [a] find a solution for the set of equations F (this is the first converged point of the line), [b] calculate the sensitivity vector dX/dS_{spec} [Eq. (13)], [c] choose a expression for function $g_{spec}(T, P, x_1, y_2, \upsilon_x, \upsilon_y, \upsilon_o)$ based on the sensitivity vector, [d] set a new value for parameter S_{spec} ($S_{spec} = S_{\text{next point}}$), [e] predict the new solution from the new S_{spec} value and from the sensitivity vector [Eq. (14)], [f] go to step [a] so as to find a new point of the SFF line.

4. Results and discussion

To evaluate the performance of the present NCM we consider a couple of base cases. The first one corresponds to the system CO_2 + n-eicosane (n-$C_{20}H_{42}$) and the second to the system CO_2 + progesterone. Each system is characterized by a base set of values for the parameters of the model. The parameterization strategy for the base cases is described in Appendix B (see supplementary material). For a given system, we impose a perturbation on the value of the $\Delta\upsilon^{S-L}$ parameter and observe how the SFF lines change. In this way we obtain SFF lines of widely varying shapes and degrees of non linearity. Finally, we establish whether the NCM is able to completely track such SFF lines of varying nature. When we perturbate the $\Delta\upsilon^{S-L}$ parameter with respect to its base value, the model departs from the experimental data. The reader is asked to understand that the scope of the present work is the definition of robust calculation procedures rather than the evaluation of the model quantitative performance. Only the parameter values used for the "base cases" correlate to experimental data. In other words, we focus in this work on the definition of calculation proce-

Table 2
Properties of pure compounds.

Compound	T_{tp} (K)	P_{tp} (bar)	T_{crit} (K)	P_{crit} (bar)	ω
CO_2			304.21[a]	73.83[a]	0.223621[a]
			304.1[b]	73.8[b]	0.239[b]
n-Eicosane	309.58[a]	$2.10470817 \times 10^{-7}$	768[a]	11.60[a]	0.906878[a]
Progesterone	406.11[c]	$1.56246138 \times 10^{-4}$	932.3[b]	19.2[b]	0.52[b]

T_{crit} = Critical temperature. P_{crit} = Critical pressure. ω = Acentric factor. P_{tp} = PR-EOS pure compound vapor–liquid equilibrium pressure at the triple point temperature T_{tp} (this work).
[a] From DIPPR database [37]: These values were used in this work for calculations for the system CO_2 + n-eicosane.
[b] From [38]: These values were used in this work for calculations for the system CO_2 + progesterone.
[c] From [33].

dures able to track, with a minimum level of user intervention, the solid–fluid–fluid equilibrium lines given by a model, once specific numerical values have been set for the model parameters.

Table 2 reports part of the pure compound characteristic constants, and Table 3 the values for the interaction parameters for the PR-EOS [34], that we used in this work. The ability of these interaction parameters to properly reproduce experimental fluid–fluid equilibrium data has already been shown in reference [36] for CO_2 + n-eicosane and in reference [33] for CO_2 + progesterone. Table 4 reports the values we used in this work for C_1, C_2, C_3 and $\Delta\upsilon^{S-L}$ (base case values of $\Delta\upsilon^{S-L}$), for n-eicosane [36] and Progesterone. Ref. [36] reports the agreement between solid–fluid equilibrium experimental data and the model, obtained with parameters from Tables 2–4, for the system CO_2 + n-eicosane. We obtained the value of $\Delta\upsilon^{S-L}$ of Table 4 for pure Progesterone, from experimental mixture solid–fluid equilibrium data from reference [33], and next computed C_1 (see details in Appendix B within the supplementary material). Fig. 8(f) shows, among other lines, the calculated solid–liquid equilibrium line (melting curve) for pure n-eicosane, which is in good agreement with experimental data up to a pressure of about 900 bar, as shown in reference [36]. Similarly, Figs. 13 and 14 show, together with other information, the calculated melting curve for pure Progesterone. This curve matches the Progesterone triple point temperature reported in Table 2.

Fig. 7 shows the calculated pressure–temperature projection of univariant lines corresponding to the fluid phase behavior for the CO_2 + n-$C_{20}H_{42}$ system, without accounting for the interference of solids. We see the vapor–liquid equilibrium lines for pure CO_2 (see inset) and pure n-$C_{20}H_{42}$, a binary critical line that originates at the pure n-$C_{20}H_{42}$ critical point, a critical line stemming from the pure CO_2 critical point (inset) which ends at an upper critical end point, and a binary liquid–liquid–vapor line (inset). Fig. 7 was obtained according to Ref. [30] and corresponds to the type III fluid phase behavior according to the classification of Scott and van Konynenburg [7]. One or more of the binary lines of Fig. 7 will be affected if, in the model, we allow the precipitation of pure n-$C_{20}H_{42}$ in solid state.

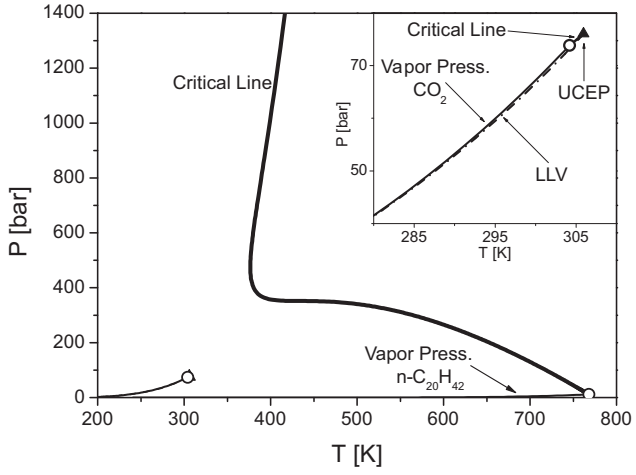

Fig. 7. Calculated pressure–temperature projection of univariant lines corresponding to the fluid phase behavior for the CO_2 + n-$C_{20}H_{42}$ system. Lines: PR-EOS with parameters from Tables 2 and 3. Circle: calculated pure compound critical point. ▲: calculated UCEP. The interference of solids is not accounted for in this figure.

Fig. 8 shows the evolution of the calculated phase behavior for the system CO_2 + n-$C_{20}H_{42}$, involving fluid and solid phases, as parameter $\Delta\upsilon^{S-L}$ changes in the range from $\Delta\upsilon^{S-L} = -0.052547\ m^3/kmol$ to $\Delta\upsilon^{S-L} = -0.238\ m^3/kmol$. The base case ($\Delta\upsilon^{S-L} = -0.072548\ m^3/kmol$, Table 4), i.e., the one that matches experimental information [36], is depicted in Fig. 8(b). At $\Delta\upsilon^{S-L} = -0.052547\ m^3/kmol$ [Fig. 8(a)], the LLV line is interrupted by a quadruple point of the S_2LLV type, whose temperature is about 296 K. Three SFF lines stem from the Q-Point, all of them calculated according to the procedure described in items IV to VI. If we decrease the value of $\Delta\upsilon^{S-L}$ to $\Delta\upsilon^{S-L} = -0.072548\ m^3/kmol$ [base case, Fig. 8(b)], the Q-point is shifted to a temperature of about 300 K, which matches the experimental Q-point temperature [36]. In this case the stable segment of the LLV line is shorter

Table 3
Binary interaction parameters for the PR-EOS.

System	k_{ij}	l_{ij}	Source
CO_2 + n-Eicosane	0.0933	0.0054	Rodriguez-Reartes et al. [36]
CO_2 + Progesterone	0.022	−0.0617	Favareto et al. [33]

Table 4
n-Eicosane and progesterone constants for Eq. (2).

Parameter	n-Eicosane[a]	Progesterone
$\Delta\upsilon^{S-L}$[b] ($m^3/kmol$)	−0.0725476936 (base case)	−0.156300841[c] (base case)
Δh^f (J/g)	–	99.18[d]
C_1 (bar)	−11688.9617	−1995.3919[c]
C_2 (bar)	34047.5683	0.0
C_3 (bar)	−70535.1757	0.0

[a] Parameter values from [36].
[b] The $\Delta\upsilon^{S-L}$ values in this table are "base values" for our parametric studies for the systems CO_2 + n-Eicosane and CO_2 + Progesterone.
[c] Obtained in this work.
[d] From [33].

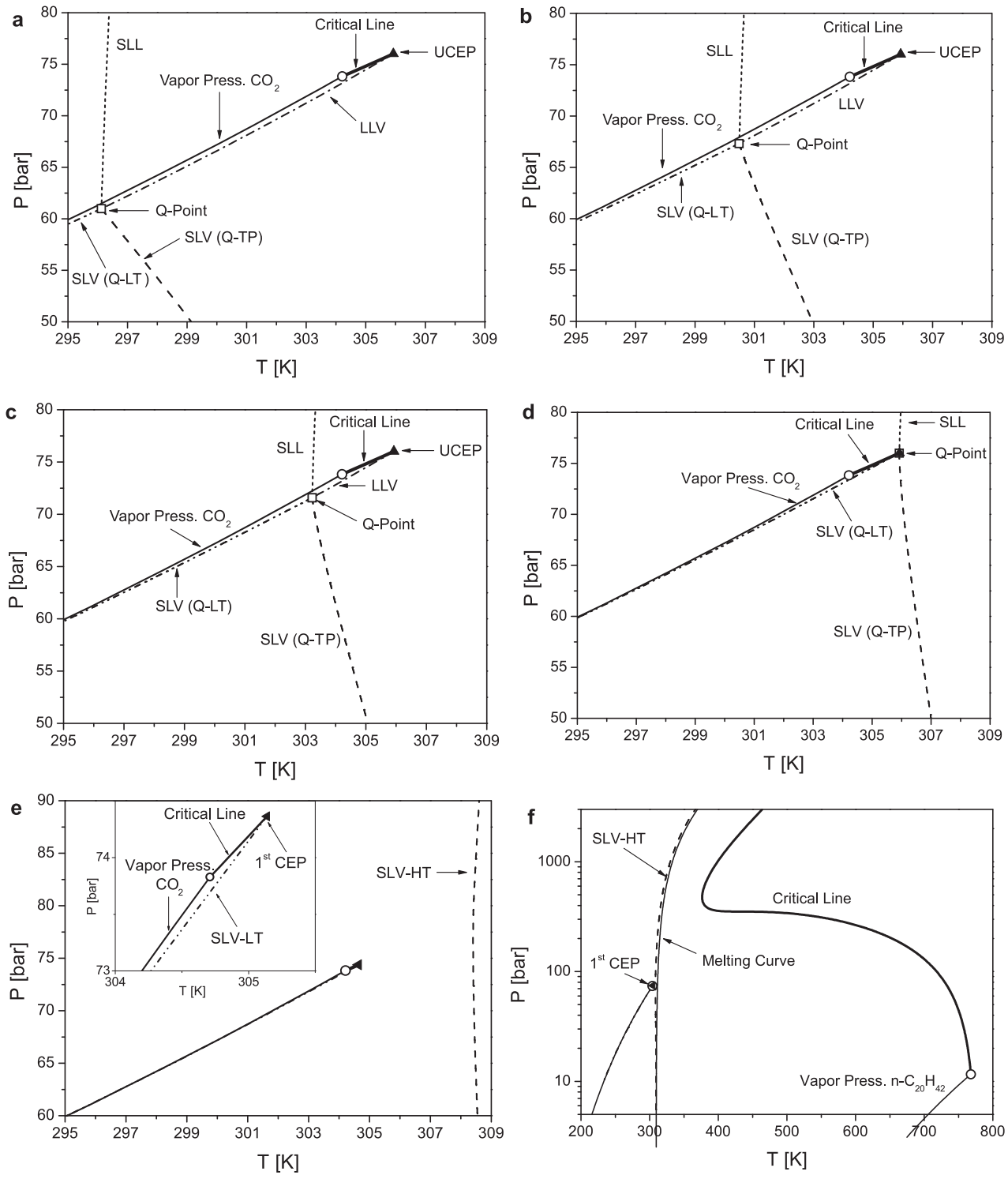

Fig. 8. Evolution of the calculated Q point (□) with the change of the parameter $\Delta\upsilon^{S-L}$ for the system CO_2 + n-$C_{20}H_{42}$. Each calculated three-phase line that stems from the quadruple point is also shown on each chart. (a): $\Delta\upsilon^{S-L} = -0.052547\,m^3/kmol$. (b): $\Delta\upsilon^{S-L} = -0.072548\,m^3/kmol$ (base case). (c): $\Delta\upsilon^{S-L} = -0.095255\,m^3/kmol$. (d): $\Delta\upsilon^{S-L} = -0.138\,m^3/kmol$: in this chart, the *PT* coordinates of the Q-point and the UCEP almost coincide. (e): $\Delta\upsilon^{S-L} = -0.238\,m^3/kmol$: in this chart we observe a 1st CEP and no Q-Point. A 2nd CEP appears beyond the scale of the chart. (f): projection in a wider *PT* range than for (e), for the CO_2 + n-$C_{20}H_{42}$ system with $\Delta\upsilon^{S-L} = -0.238\,m^3/kmol$. Symbols: circle: pure compound critical point. ▲ UCEP. ◄ 1st CEP. □: Q-Point. All univariant lines and non-variant points correspond to the PR-EOS for the fluid phases and to Eq. (1) for the pure solid n-$C_{20}H_{42}$. The parameter values are reported in Tables 2–4 except for $\Delta\upsilon^{S-L}$, which is variable in this set of charts. The calculated background fluid phase behavior is available in Fig. 7. Fig. 8(a)–(d) correspond to the Type E behavior schematically shown in Fig. 5, while Fig. 8(e) and (f) correspond to the Type F of Fig. 6.

than for Fig. 8(a). The SFF lines are shifted together with the Q-Point. A further decrease of $\Delta\upsilon^{S-L}$ to $\Delta\upsilon^{S-L} = -0.095255\,m^3/kmol$ [Fig. 8(c)], makes such segment become even shorter. The type of phase behavior that Fig. 8(a)–(c) shows, has been experimentally observed, e.g., for the systems considered in refs [19–21]. For an even lower value for $\Delta\upsilon^{S-L}$ such that $\Delta\upsilon^{S-L} = -0.138\,m^3/kmol$ [Fig. 8(d)], the *PT* coordinates of the Q-point become almost coincident with those of the UCEP. Finally, at $\Delta\upsilon^{S-L} = -0.238\,m^3/kmol$ [Fig. 8(e) and (f)], the SLL line and the SLV(Q-TP) line become a single line that ends at a (not shown) 2nd CEP (SLV-HT line) and

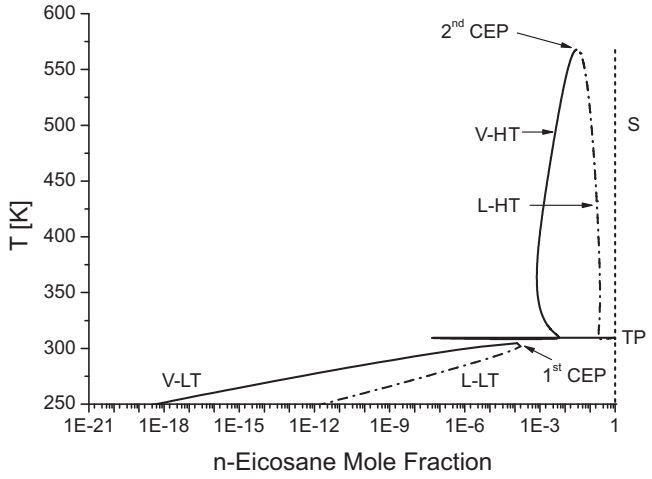

Fig. 9. Temperature–composition projection of calculated solid–fluid–fluid equilibrium lines for the system CO_2 + n-$C_{20}H_{42}$. $\Delta\upsilon^{S-L} = -0.238\ m^3/kmol$. Lines: model. The lines corresponding to the phases at SLV equilibrium for the SLV line that goes from the 1st CEP to low temperature (SLV-LT) are: low temperature vapor (V-LT), low temperature liquid (L-LT), and pure solid (S). The lines corresponding to the phases at SLV equilibrium for the SLV line that goes from the triple point (TP) to the 2nd CEP (SLV-HT) are: high temperature vapor (V-HT), high temperature liquid (L-HT), and pure solid (S). Both SFF lines correspond to the PR-EOS for the fluid phases and to Eq. (1) for the pure solid n-$C_{20}H_{42}$. The parameter values are reported in Tables 2–4 except for $\Delta\upsilon^{S-L}$. This figure corresponds to the Type F behavior schematically shown in Fig. 6.

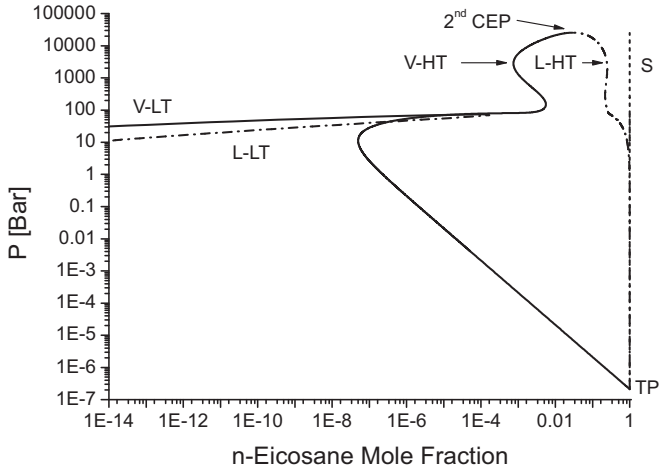

Fig. 10. Pressure–composition projection of calculated solid–fluid–fluid equilibrium lines for the system CO_2 + n-$C_{20}H_{42}$. $\Delta\upsilon^{S-L} = -0.238\ m^3/kmol$. Lines: model (labels as in Fig. 9). Both SFF lines correspond to the PR-EOS for the fluid phases and to Eq. (1) for the pure solid n-$C_{20}H_{42}$. The parameter values are reported in Tables 2–4 except for $\Delta\upsilon^{S-L}$. This figure corresponds to the Type F behavior schematically shown in Fig. 6.

the SLV (Q-LT) line becomes a line that ends at a 1st CEP (SLV-LT line, see inset). Notice that the information shown in Fig. 8(e) is also presented in Fig. 8(f), which covers a wider *PT* range than Fig. 8(e). In Fig. 8(f), we also see the calculated critical line that originates at the pure n-$C_{20}H_{42}$ critical point, and the calculated pure n-$C_{20}H_{42}$ solid–liquid equilibrium line (melting curve). This line remains invariant with respect to $\Delta\upsilon^{S-L}$ if we keep constant the values for C_1, C_2 and C_3, as we did while generating Fig. 8 (see Appendix B for more details, in the supplementary material). Since the calculated fluid phase equilibrium is independent from $\Delta\upsilon^{S-L}$, the background fluid phase behavior is the same than that of Fig. 7, for Fig. 8(a)–(f). Notice that Fig. 8(a)–(d) correspond to the Type E behavior schematically shown in Fig. 5, while Fig. 8(e) and (f) correspond to the Type F of Fig. 6. The evolution of phase behavior that Fig. 8 shows is consistent with the progression that de Loos [14] has schematically shown for a system with a background fluid phase behavior of type III (in the classification of Scott and van Konynenburg [7]) which suffers the interference of the pure heavy component solid phase.

Figs. 9 and 10 show, respectively, the Temperature–Composition projection and the Pressure–Composition projection of the calculated SFF equilibrium curves ($\Delta\upsilon^{S-L} = -0.238\ m^3/kmol$) whose PT projections were shown in Fig. 8(f). The shallow minimum in temperature observed in Fig. 8(e) for the SLV-HT line corresponds to the loop observed (with some effort) in a very narrow temperature range, in Fig. 9, for the vapor phase (V-HT) of such line. Figs. 9 and 10 show that the point where the V-HT vapor phase and the L-HT liquid phase become identical, i.e., the 2nd CEP, is very closely approached by the NCM here proposed. Convergence problems may arise in the neighborhood of critical end points or of loops, when conventional methods (not having a numerical continuation nature) are used. This requires a considerable amount of user intervention, for finding the three-phase equilibrium solutions. Such problem is avoided by applying NCMs as the one here proposed.

Notice, in Fig. 9, that the n-Eicosane mole fraction is very low at the lowest temperature (250 K) for the vapor phase (V-LT) and for the liquid phase (L-LT) which are both at equilibrium with pure solid n-Eicosane (S). Such mole fraction values are in the order of 10^{-18} for the V-LT phase and of 10^{-12} for the L-LT phase. Garcia and Luks ([12], p. 99, p. 102) have reported difficulties for computing S_2LV lines as the one with phases V-LT and L-LT in Fig. 9. We attribute the successful calculation, in a fairly wide temperature range, of such line in Fig. 9, to our use of a NCM, to the logarithmic scaling of the system variables and to having obtained a first converged point as explained in Appendix A. The lowest temperature in Fig. 9 (250 K) corresponds to a very low reduced temperature ($T_r = 0.33$) for the heavy compound (see Table 2).

Fig. 11 shows the calculated pressure–temperature projection of univariant lines corresponding to the fluid phase behavior for the CO_2 + progesterone system, without accounting for the interference of solids. Fig. 11 was obtained according to Ref. [30]. In this figure, the inset facilitates the observation of the phase behavior at low temperature. The phase diagram of Fig. 11 corresponds to type II phase behavior in the classification of Scott and van Konynenburg [7].

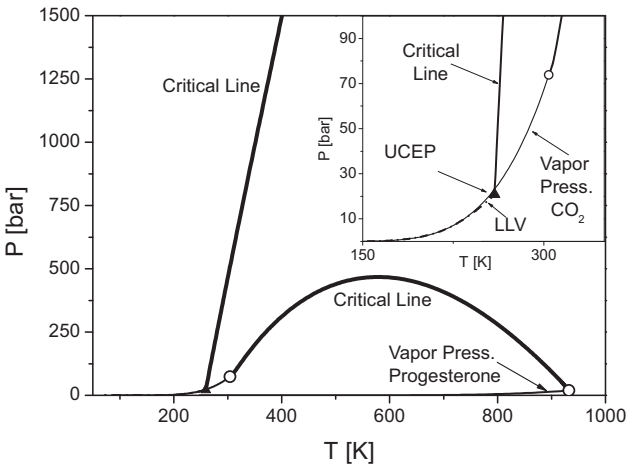

Fig. 11. Calculated pressure–temperature projection of univariant lines corresponding to the fluid phase behavior for the CO_2 + progesterone system. Lines: PR-EOS with parameters from Tables 2 and 3. Symbols: circle: calculated pure compound critical point. ▲ calculated UCEP. The interference of solids is not accounted for in this figure.

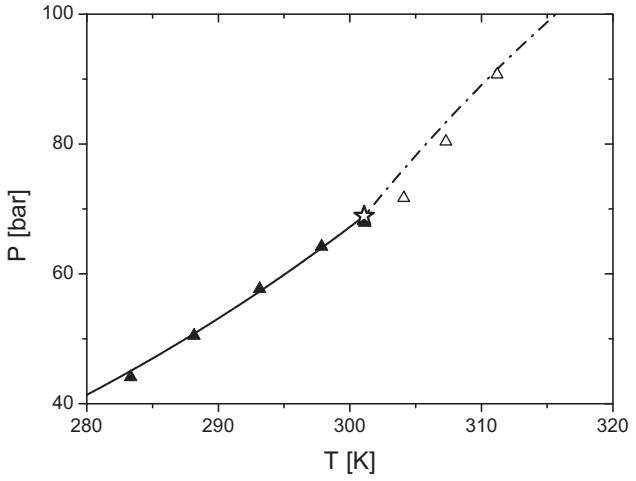

Fig. 12. Isopleth phase envelope portion, for the system CO_2 + progesterone, for a mole fraction of progesterone (X_{Prog}) equal to 0.00014. Experimental data [33]: ▲: liquid–vapor equilibrium, empty triangles: solid–fluid equilibrium. Modeling results obtained with the PR-EOS for the fluid phases and Eq. (1) for the pure solid progesterone. Model parameters from Tables 2–4. Calculated isoplethic equilibrium segments: (—) liquid–vapor equilibrium, (– . – . –) solid–fluid equilibrium. Star: calculated SLV equilibrium point.

Fig. 12 presents part of the phase envelope of an isopleth for the system CO_2 + progesterone corresponding to a mole fraction of progesterone (X_{Prog}) equal to 0.00014. The solid and empty triangles correspond, respectively, to liquid–vapor equilibrium and solid–fluid equilibrium experimental data from Ref [33]. The lines are model calculations with parameters from Tables 2–4. Fig. 12 corresponds to our "base value" for $\Delta\upsilon^{S-L}$, i.e., to $\Delta\upsilon^{S-L} = -0.156300841\ m^3/kmol$ (Table 4). We see an acceptable agreement between the model and the experiments. However, matching experimental data is beyond the scope of this work, which deals with the definition and testing of robust calculation procedures.

Fig. 13 shows the evolution of the calculated CO_2 + progesterone SLV equilibrium line stemming from the pure Progesterone triple

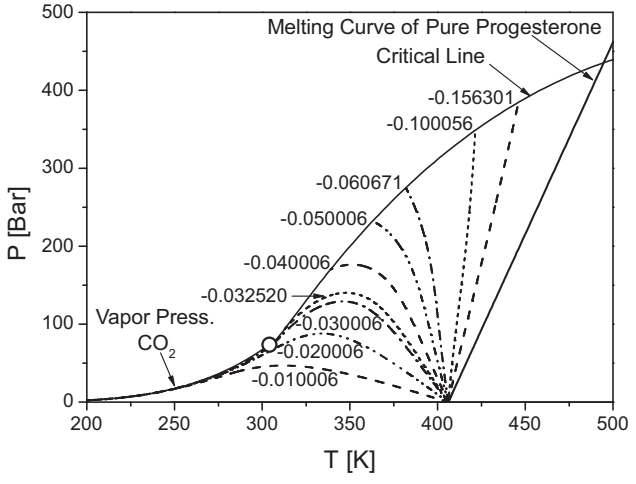

Fig. 13. Evolution of the calculated CO_2 + progesterone SLV equilibrium line stemming from the pure Progesterone triple point, as parameter $\Delta\upsilon^{S-L}$ increases: Calculated *PT* projection of phase equilibrium univariant lines. The $\Delta\upsilon^{S-L}$ values are given on the chart and have m^3/kmol units. The base case is the one with $\Delta\upsilon^{S-L} = -0.156301$ (Table 4). Circle: calculated pure CO_2 critical point. Model: PR-EOS for the fluid phases and Eq. (1) for the pure solid Progesterone. Model parameters from Tables 2–4 except for $\Delta\upsilon^{S-L}$. The calculated background fluid phase behavior is available in Fig. 11. Depending on the value of $\Delta\upsilon^{S-L}$ the behavior corresponds in this figure either to type A (Fig. 1) or to Type F (Fig. 6).

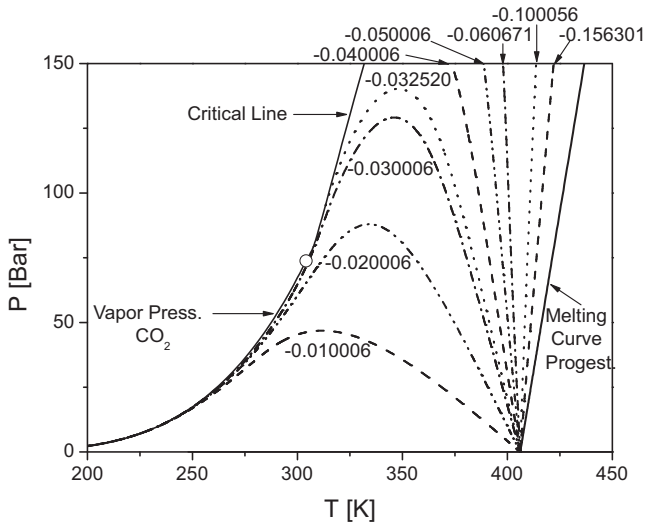

Fig. 14. Evolution of the calculated CO_2 + progesterone SLV equilibrium line stemming from the pure Progesterone triple point, as parameter $\Delta\upsilon^{S-L}$ increases: Calculated *PT* projection of phase equilibrium univariant lines. The $\Delta\upsilon^{S-L}$ values are given on the chart and have m^3/kmol units. The base case is the one with $\Delta\upsilon^{S-L} = -0.156301$ (Table 4). Circle: calculated pure CO_2 critical point. Model: PR-EOS for the fluid phases and Eq. (1) for the pure solid Progesterone. Model parameters from Tables 2–4, except for $\Delta\upsilon^{S-L}$. The calculated background fluid phase behavior is available in Fig. 11. Depending on the value of $\Delta\upsilon^{S-L}$ the behavior corresponds in this figure either to type A (Fig. 1) or to Type F (Fig. 6).This figure shows the same information than Fig. 13, but in a narrower pressure range, for visualization purposes.

point, as parameter $\Delta\upsilon^{S-L}$ increases starting from its base value (i.e., from $\Delta\upsilon^{S-L} = -0.156300841\ m^3/kmol$). Fig. 14 shows the same information than Fig. 13, but in a narrower pressure range, for visualization purposes.

The behavior corresponds in Figs. 13 and 14 to Type F (Fig. 6) for low enough values of $\Delta\upsilon^{S-L}$ and to type A (Fig. 1) for high enough values of $\Delta\upsilon^{S-L}$. The transition from Type F to type A behavior happens at a $\Delta\upsilon^{S-L}$ value ($\Delta\upsilon^{S-L}_{trans}$) such that $-0.032520\ m^3/kmol < \upsilon^{S-L}_{trans} < -0.030006\ m^3/kmol$. At $\Delta\upsilon^{S-L} = \Delta\upsilon^{S-L}_{trans}$, the SLV line intersects the critical line at a point where both lines have a common tangent line. For $\Delta\upsilon^{S-L}$ values corresponding to type F behavior, Figs. 13 and 14 show only SLV lines that end at a 2nd CEP. Fig. 15 complements such information by showing SLV lines stemming from a 1st CEP. Fig. 15 shows that the 1st CEP gets closer to the pure CO_2 critical point as parameter $\Delta\upsilon^{S-L}$ becomes more negative.

The calculated background fluid phase behavior is not affected by parameter $\Delta\upsilon^{S-L}$ and therefore remains invariant (i.e., equal to that of Fig. 11) at all conditions shown in Figs. 13–15. However, the interference of solid Progesterone makes part of the vapor–liquid critical line become unstable, if $\Delta\upsilon^{S-L}$ has a value such that the behavior is of type F (Fig. 6). For a given $\Delta\upsilon^{S-L}$ value, the unstable part of the critical line is the one that connects the 1st CEP with the 2nd CEP and, also, the liquid–liquid critical line and the liquid–liquid–vapor line are unstable. For a better understanding we include Fig. 16 which presents the calculated *PT* projection of phase equilibrium univariant lines for the system CO_2 + progesterone with $\Delta\upsilon^{S-L} = -0.050006\ m^3/kmol$. We see two different critical loci, both lying on the same background vapor–liquid critical line shown in Fig. 11. One of the critical loci starts at the critical point of pure CO_2 and ends at a 1st CEP (see the inset in Fig. 16), and the other critical locus goes from the critical point of pure progesterone to the 2nd CEP.

Notice that our $\Delta\upsilon^{S-L}$ "base value" ($\Delta\upsilon^{S-L} = -0.156300841\ m^3/kmol$, Table 4) for the system CO_2 + progesterone, which comes from reproducing fluid–fluid

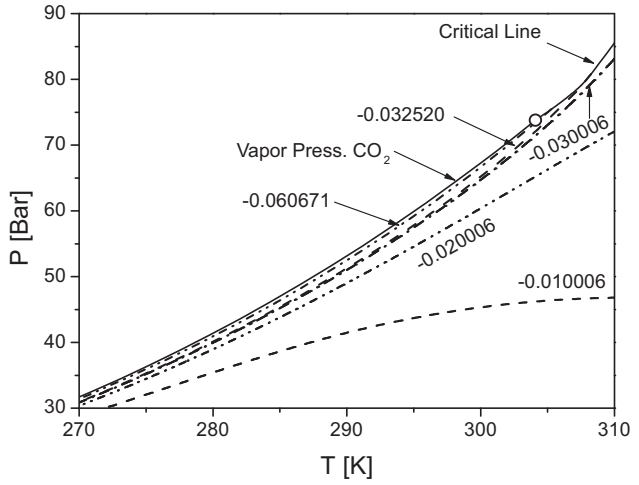

Fig. 15. Evolution, in a narrow temperature range, of the calculated CO_2 + progesterone SLV equilibrium lines as parameter $\Delta\upsilon^{S-L}$ increases: Calculated *PT* projection of phase equilibrium univariant lines. The $\Delta\upsilon^{S-L}$ values are given on the chart and have m^3/kmol units. Model: PR-EOS for the fluid phases and Eq. (1) for the pure solid Progesterone. Circle: calculated pure CO_2 critical point. Model parameters from Tables 2–4, except for $\Delta\upsilon^{S-L}$. The calculated background fluid phase behavior is available in Fig. 11. Depending on the value of $\Delta\upsilon^{S-L}$ the behavior corresponds in this figure either to type A (Fig. 1) or to Type F (Fig. 6). Some of the shown SLV lines stem from the pure Progesterone triple point while others originate at a 1st CEP. This figure shows that the 1st CEP gets closer to the pure CO_2 critical point as parameter $\Delta\upsilon^{S-L}$ becomes more negative.

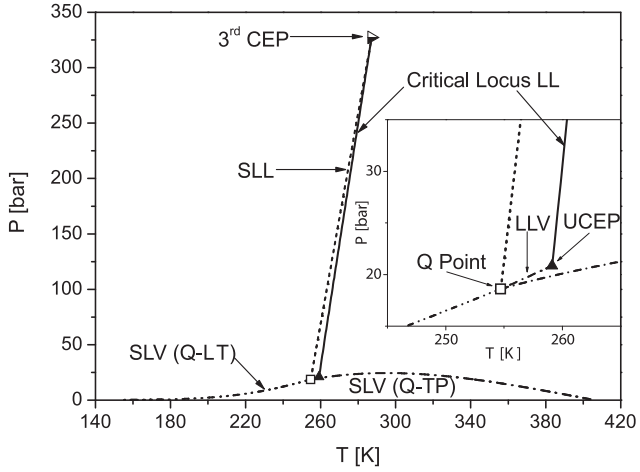

Fig. 17. Calculated *PT* projection of phase equilibrium univariant lines for the system CO_2 + Progesterone with $\Delta\upsilon^{S-L} = -0.005006\ m^3$/kmol. The nature of each curve is indicated on the chart. Symbols: ▲Calculated UCEP. □: Calculated Q-Point. Half-full triangle: calculated 3rd CEP. Model: PR-EOS for the fluid phases and Eq. (1) for the pure solid Progesterone. Model parameters from Tables 2–4 except for $\Delta\upsilon^{S-L}$. The calculated background fluid phase behavior is available in Fig. 11. The behavior corresponds in this figure to Type C which Fig. 3 schematically shows.

and solid–fluid experimental information from Ref. [33], together with parameters for the PR-EOS from the same Ref. [33], leads to the conclusion that the system CO_2 + progesterone has an experimental behavior corresponding to type F (Fig. 6) in the classification of Yamamoto et al. [9], and a background fluid phase behavior of type II (Fig. 11) in the classification of van Konynenburg and Scott [7] [8]. We have achieved these conclusions thanks to the numerical continuation methods (NCMs) proposed previously [30] for computing univariant fluid phase equilibrium lines and to the NCM here proposed for calculating complete SFF lines.

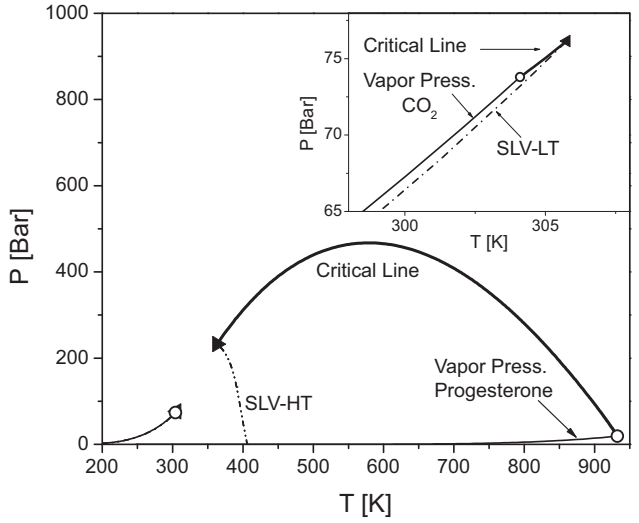

Fig. 16. Calculated *PT* projection of phase equilibrium univariant lines for the system CO_2 + progesterone with $\Delta\upsilon^{S-L} = -0.050006\ m^3$/kmol. Circle: calculated pure compound critical point. ◂: 1st CEP. ▷: 2nd CEP. Model: PR-EOS for the fluid phases and Eq. (1) for the pure solid Progesterone. Model parameters from Tables 2–4 except for $\Delta\upsilon^{S-L}$. The calculated background fluid phase behavior is available in Fig. 11. The behavior corresponds in this figure to Type F which Fig. 6 schematically shows.

It is worth noting that the authors of Refs. [18,22,23] concluded, from the experimental data there reported, that their studied systems had a type F phase behavior, with a temperature minimum for the SFF locus that goes from the TP of the heavy compound to the 2nd CEP. Refs. [18,22,23] do not present modeling results for the SFF loci. Such lack of modeling results might be related to difficulties in the computation of the SFF lines due to the highly non-linear nature that SFF loci of type F systems may have, as illustrated in, e.g., Figs. 9 and 10.

For $\Delta\upsilon^{S-L}$ values sufficiently above the maximum value of Figs. 14 and 15, i.e., if $\Delta\upsilon^{S-L}$ is sufficiently greater than $-0.010006\ m^3$/kmol, then, the LLV line of Fig. 11 becomes stable between the UCEP and a point where the LLV line suffers the interference of solid progesterone. Similarly, the liquid–liquid critical line becomes stable between the UCEP and the 3rd CEP. This is illustrated in Fig. 17 which shows the calculated PT projection of phase equilibrium univariant lines for the system CO_2 + progesterone at $\Delta\upsilon^{S-L} = -0.005006\ m^3$/kmol. Such behavior corresponds to the Type C pattern which Fig. 3 schematically shows. The interference by solid progesterone, that Fig. 17 shows, causes the appearance of a quadruple point (Q-point). From that point, four three-phase equilibrium curves emerge: (1) a SLL equilibrium curve that goes to high pressure and ends at a 3rd CEP; (2) a SLV curve connecting the Q-point to the TP of the heavy compound; (3) a SLV curve that extends toward low temperatures; and, (4), the LLV equilibrium line ending at the UCEP. Fig. 18 corresponds to $\Delta\upsilon^{S-L} = -0.003506\ m^3$/kmol, i.e., to a $\Delta\upsilon^{S-L}$ value more positive, and closer to zero, than that of Fig. 17. This implies a size increase for the stable part of the LLV line, i.e., as $\Delta\upsilon^{S-L}$ approaches to zero, the Q-point is shifted (along the background LLV line of Fig. 11) to lower temperatures, while the 3rd CEP goes to higher pressures (along the background LL critical line of Fig. 11. See Figs. 17 and 18). In Fig. 18 the 3rd CEP is not shown: it appears at pressures higher than 400 bar.

Now we come back to the range of variation for $\Delta\upsilon^{S-L}$ of Fig. 13, i.e., from $\Delta\upsilon^{S-L} = -0.156301\ m^3$/kmol (base case, Table 4) to $\Delta\upsilon^{S-L} = -0.010006\ m^3$/kmol, and present, in Fig. 19, the evolution of the lines showing the mole fraction of Progesterone in the liquid phase (X_{Prog}) vs. the mole fraction of progesterone in the vapor phase (Y_{Prog}), under SLV equilibrium conditions,

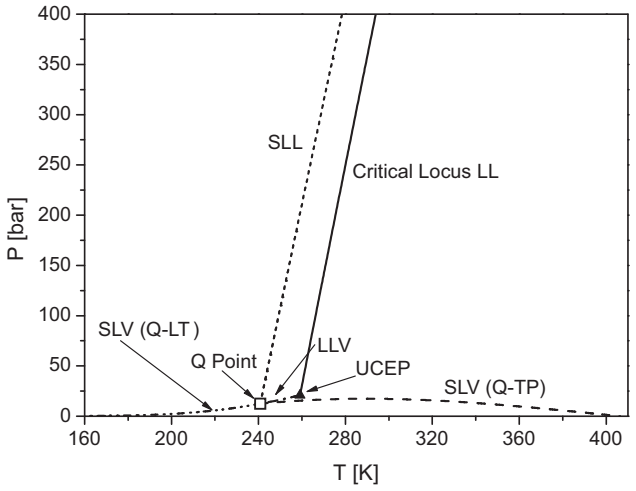

Fig. 18. Calculated *PT* projection of phase equilibrium univariant lines for the system CO_2 + Progesterone with $\Delta\upsilon^{S-L} = -0.003506\,m^3/kmol$. The nature of each curve is indicated on the chart. Symbols: ▲ Calculated UCEP. □: Calculated Q-Point. Model: PR-EOS for the fluid phases and Eq. (1) for the pure solid Progesterone. Model parameters from Tables 2–4 except for $\Delta\upsilon^{S-L}$. The calculated background fluid phase behavior is available in Fig. 11. The behavior corresponds in this figure to Type C which Fig. 3 schematically shows.

calculated for the system CO_2 + progesterone. For the base case [$\Delta\upsilon^{S-L} = -0.156301\,m^3/kmol$, Fig. 19(a)], we see two SFF lines (Type F behavior, Fig. 6). One of them starts at the point with coordinates $X_{Prog} = 1$ and $Y_{Prog} = 1$, i.e., at the TP of pure progesterone, and ends at a point on the auxiliary identity line (dashed line). Such point corresponds to the 2nd CEP where both fluid phases have identical composition. The other line starts at the 1st CEP which, clearly, also belongs to the identity line. As $\Delta\upsilon^{S-L}$ increases [$\Delta\upsilon^{S-L} = -0.032520\,m^3/kmol$, Fig. 19(b)], the 1st CEP and the 2nd CEP get closer. A further increase in $\Delta\upsilon^{S-L}$ [$\Delta\upsilon^{S-L} = -0.030006\,m^3/kmol$, Fig. 19(c)], makes both SFF lines become a (highly non-linear) single curve. This is associated to the disappearance of the 1st and 2nd CEPs (type A behavior, Fig. 1). Fig. 19(b) and (c) shows, much more clearly than Figs. 13–15, that the transition from Type F [Fig. 19(b)] to type A [Fig. 19(c)] happens at a $\Delta\upsilon^{S-L}$ value ($\Delta\upsilon^{S-L}_{trans}$) such that $-0.032520\,m^3/kmol < \Delta\upsilon^{S-L}_{trans} < -0.030006\,m^3/kmol$, as previously stated. A further increase in $\Delta\upsilon^{S-L}$ such that $\Delta\upsilon^{S-L}$ is sufficiently greater than $\Delta\upsilon^{S-L}_{trans}$ [$\Delta\upsilon^{S-L} = -0.010006\,m^3/kmol$, Fig. 19(d)] produces a monotonically increasing line with a behavior simpler than that of the single line of Fig. 19(c).

In Appendix C (supplementary material) we present a number of Pressure–Composition and Temperature–Composition projections

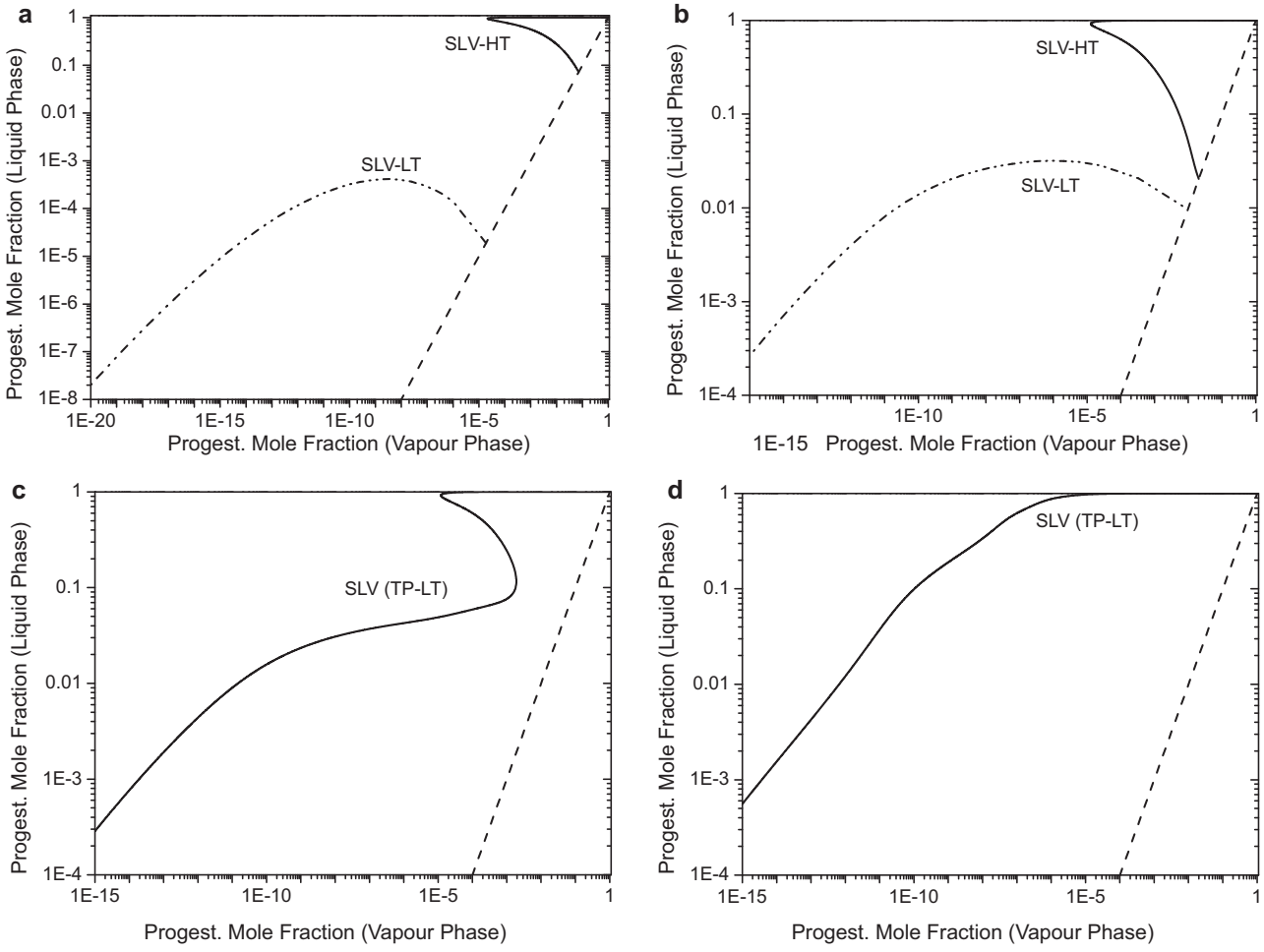

Fig. 19. Mole fraction of Progesterone in the liquid phase (X_{Prog}) vs. mole fraction of Progesterone in the vapor phase (Y_{Prog}), under SLV equilibrium conditions, calculated for the system CO_2 + progesterone. Evolution of the calculated X_{Prog} vs. Y_{Prog} lines as parameter $\Delta\upsilon^{S-L}$ increases. (a): $\Delta\upsilon^{S-L} = -0.156301\,m^3/kmol$ (base case, Table 4). (b): $\Delta\upsilon^{S-L} = -0.032520\,m^3/kmol$. (c): $\Delta\upsilon^{S-L} = -0.030006\,m^3/kmol$. (d): $\Delta\upsilon^{S-L} = -0.010006\,m^3/kmol$. The dashed line is the identity curve, and it was included on each chart to allow a better understanding. Model: PR-EOS for the fluid phases and Eq. (1) for the pure solid Progesterone. Model parameters from Tables 2–4, except for $\Delta\upsilon^{S-L}$. The calculated background fluid phase behavior is available in Fig. 11. Depending on the value of $\Delta\upsilon^{S-L}$ the behavior corresponds in this figure either to type A (Fig. 1) or to Type F (Fig. 6).

of calculated solid–liquid–vapor (SLV) equilibrium curves for the system CO_2 + progesterone for varying values of the $\Delta\upsilon^{S-L}$ parameter. Some of such projections clearly illustrate the highly non-linear behavior that SFF hyper lines may have.

In Appendix D (supplementary material), we show for a particular SFF line, the evolution of the choice of the specified variable as the computation of the SFF line progresses. Such sample SFF line extends from the TP of the heavy compound to an indefinitely low temperature. From Fig. 22 of Appendix D, it is clear that the choice of pressure or temperature as the specified variable, for all points of the SFF line to be built, based on the expected shape of PT projection of the SFF locus, may not be (and in general will not be) optimum, on top of forcing the user to guess the shape of the SFF curve. The SFF line considered in Appendix D corresponds to a type A system. It is a difficult to compute line if we do not resort to a NCM. Type A behavior was found in the laboratory for, e.g., the system propane + eicosane [17]. Fig. 23 within Appendix D (supplementary material) is very important for understanding how the NCM selects the variable to be specified as the calculation of the SFF line progresses.

From the results presented, it is clear that the present NCM is able to track complete SFF lines of varied nature, from well-behaved lines to highly curved ones.

5. Remarks and conclusions

Numerical continuation methods (NCMs) are inherently robust and therefore make it possible to minimize the level of user intervention when tracking highly non-linear curves. In this work, we have proposed, described and tested a NCM for calculating solid–fluid–fluid equilibrium loci, of varying shape and degree of non-linearity, for binary asymmetric systems, over wide ranges of conditions. Examples of computations that may be difficult to complete, without using a NCM, are illustrated in figures such as Fig. 20(b) and (c) of the supplementary material accompanying this article. The present NCM is able to solve SFF equilibria even at conditions quite close to those of critical end points where a critical fluid phase is at equilibrium with a solid phase. Every SFF equilibrium line was calculated in this work in a single run, regardless the degree o non-linearity of the computed SFF locus.

Among other algorithms, we have proposed in this work a special procedure (see item III of section 3.5 and Appendix A) to obtain SFF lines that have been previously regarded as difficult to compute [12]. This is related to the very low concentration of the heavy component of the binary asymmetric system in either fluid phase, at SFF conditions, at low temperature.

Although we have made, for illustration purposes, particular choices for the equation of state that represents the properties of the fluid phases and for the description of the solid fugacity, the present NCM is of general applicability.

We have considered in this work the asymmetric systems Carbon Dioxide + n-Eicosane and Carbon Dioxide + Progesterone. In this last case, we have illustrated the usefulness of the proposed NCM for characterizing the behavior of the system CO_2 + progesterone from limited, recently obtained [33], isoplethic fluid–fluid and solid–fluid experimental equilibrium data. For the system Carbon Dioxide + n-Eicosane, the base set of parameters was obtained through a technique, described in Appendix B (supplementary material), that leaves invariant the description of the pure n-Eicosane melting curve (and also of the mixture fluid–fluid equilibria) while fitting mixture solid–fluid equilibrium data.

SFF equilibrium lines provide, together with other univariant lines (critical, liquid–liquid–vapor, azeotropic), key points for isothermal or isobaric or constant-composition cuts of the equilibrium surfaces that relate the temperature, the pressure and the phase compositions. Therefore, it is important to have available robust calculation procedures for computing SFF lines, as the one presented in this work.

Acknowledgements

We are grateful, for their financial support, to Consejo Nacional de Investigaciones Científicas y Técnicas (CONICET, Argentina), Universidad Nacional del Sur (U.N.S., Argentina), Universidad Nacional de Córdoba (U.N.C., Argentina) and Agencia Nacional de Promoción Científica y Tecnológica (ANPCyT, Argentina). We also thank Professor Lucio Cardozo-Filho of Universidade Estadual de Maringá (Brazil) for helpful discussions on the system Carbon Dioxide + Progesterone.

Appendix A. Algorithm for computing a low temperature–low pressure (LTLP) SFF point

- Set $T = T_{c,light} - 60$ K, where $T_{c,light}$ is the critical temperature of the light component.
- Let P be the calculated liquid–vapor equilibrium pressure of the pure light component, at $T = T_{c,light} - 60$ K, obtained with the *PVTx* relationship adopted to describe the fluid state, by equating pure compound fugacities in liquid and vapor state. P is used as initial estimate for the SFF pressure.
- Set υ_x and υ_y, respectively, as the liquid molar volume and the vapor molar volume of the liquid–vapor equilibrium point calculated previously for the pure light component.
- At T and P, compute the fugacity coefficient of the heavy component "2" at infinite dilution in component "1" as saturated vapor, i.e., $\hat{\phi}_2^{V,\infty}$, where $\hat{\phi}_2^{V,\infty}$ is evaluated at T and at υ_y setting $z_2 = 0$.
- At T and P, compute the fugacity coefficient of the heavy component "2" at infinite dilution in component "1" as saturated liquid, i.e., $\hat{\phi}_2^{L,\infty}$, where $\hat{\phi}_2^{L,\infty}$ is evaluated at T and at υ_x setting $z_2 = 0$.
- Compute the equilibrium ratio of component "2" at infinite dilution in the saturated component "1" as $K_2^{\infty} = \hat{\phi}_2^{L,\infty}/\hat{\phi}_2^{V,\infty}$.
- Solve the *PVTx* relationship for the pure heavy compound "2" at T and P to obtain the initial estimate for υ_o.
- At T and P, estimate the hypothetical solubility of the heavy component "2" in the light component "1" as saturated vapor (y_2^{∞}), as $y_2^{\infty} = f_2^S(T, P, \upsilon_o)/(\hat{\varphi}_2^{V,\infty} P)$. From y_2^{∞}, estimate the composition of the liquid phase (x_2^{∞}) as $x_2^{\infty} = y_2^{\infty}/K_2^{\infty}$. In this way we obtain the pair $[x_2^{\infty}, y_2^{\infty}]_{vapor\ based}$.
- At T and P, estimate the hypothetical solubility of the heavy component "2" in the light component "1" as saturated liquid (x_2^{∞}), as $x_2^{\infty} = f_2^S(T, P, \upsilon_o)/(\hat{\varphi}_2^{L,\infty} P)$. From x_2^{∞}, estimate the composition of the vapor phase (y_2^{∞}) as $y_2^{\infty} = x_2^{\infty} K_2^{\infty}$. In this way we obtain the pair $[x_2^{\infty}, y_2^{\infty}]_{liquid\ based}$.
- Then, select between the pairs $[x_2^{\infty}, y_2^{\infty}]_{vapor\ based}$ and $[x_2^{\infty}, y_2^{\infty}]_{liquid\ based}$ the one with the minimum value for x_2^{∞}, since for such pair the use of infinite dilution fugacity coefficients is more valid than for the other pair, and, next, initialize the composition of the fluid phases as $x_1 = 1 - x_2^{\infty}$ and $y_2 = y_2^{\infty}$.
- Set $g_{spec}(T, P, x_1, y_2, \upsilon_x, \upsilon_y, \upsilon_o) = \ln(T)$ as the specification function and $S_{spec} = \ln(T_{c,light} - 60\,\text{K})$ as the value for the specification parameter, and solve the system of Eqs. (3)–(9) to obtain a SFF point.

Notice that in this algorithm initial guesses for the concentration of the heavy component in the fluid phases are generated automatically.

Appendix B. Supplementary data

Supplementary data associated with this article can be found, in the online version, at doi:10.1016/j.supflu.2011.02.004.

References

[1] P.A. Monson, Molecular thermodynamics of solid-fluid and solid-solid equilibria, AIChE Journal 54 (2008) 1122–1128.
[2] D. Vazquez, G.A. Mansoori, Identification and measurement of petroleum precipitates, Journal of Petroleum Science and Engineering 26 (2000) 49–55.
[3] G.A. Mansoori, Modeling of asphaltene and other heavy organic depositions, Journal of Petroleum Science and Engineering 17 (1997) 101–111.
[4] P. Cézac, J.-P. Serin, J. Mercadier, G. Mouton, Modelling solubility of solid sulphur in natural gas, Chemical Engineering Journal 133 (2007) 283–291.
[5] J.M. Prausnitz, Molecular thermodynamics for some applications in biotechnology, The Journal of Chemical Thermodynamics 35 (2003) 21–39.
[6] S.-D. Yeo, E. Kiran, Formation of polymer particles with supercritical fluids: a review, The Journal of Supercritical Fluids 34 (2005) 287–308.
[7] P.H. van Konynenburg, R.L. Scott, Critical lines and phase equilibria in binary van der Waals mixtures, Philosophical Transactions of the Royal Society London Series A 298 (1980) 495–540.
[8] J.R. Elliott, C.T. Lira, Introductory Chemical Engineering Thermodynamics, Prentice-Hall PTR, Upper Saddle River, NJ, 1999.
[9] S. Yamamoto, K. Ohgaki, T. Katayama, Phase behavior of binary mixtures of indole or quinoxaline with CO_2, C_2H_4, C_2H_6, and CHF_3 in the critical region, The Journal of Supercritical Fluids 2 (1989) 63–72.
[10] A. Bolz, U.K. Deiters, C.J. Peters, T.W.d. Loos, Nomenclature for phase diagrams with particular reference to vapour–liquid and liquid–liquid equilibria, Pure and Applied Chemistry 70 (1998) 2233–2258.
[11] K.D. Luks, The occurrence and measurement of multiphase equilibria behavior, Fluid Phase Equilibria 29 (1986) 209–224.
[12] D.C. Garcia, K.D. Luks, Patterns of solid-fluid phase equilibria: new possibilities? Fluid Phase Equilibria 161 (1999) 91–106.
[13] J.A. Labadie, D.C. Garcia, K.D. Luks, Patterns of solid-fluid phase equilibria: II. Interplay with fluid phase criticality and stability, Fluid Phase Equilibria 171 (2000) 11–26.
[14] T.W. de Loos, On the phase behaviour of asymmetric systems: the three-phase curve solid-liquid-gas, The Journal of Supercritical Fluids 39 (2006) 154–159.
[15] M. Cismondi, M.L. Michelsen, M.S. Zabaloy, Automated generation of phase diagrams for binary systems with azeotropic behavior, Industrial & Engineering Chemistry Research 47 (2008) 9728–9743.
[16] S. Yamamoto, K. Ohgaki, T. Katayama, High-pressure phase behavior of eight binary mixtures of pyrimidine or pyrazine with carbon dioxide, ethylene, ethane or fluoroform, Journal of Chemical & Engineering Data 35 (1990) 310–314.
[17] J. Gregorowicz, T.W. De Loos, J. De Swaan Arons, The system propane + eicosane: P, T, and x measurements in the temperature range 288-358 K, Journal of Chemical & Engineering Data 37 (1992) 356–358.
[18] E. Flöter, T.W. de Loos, J. de Swaan Arons, High pressure solid-fluid and vapour-liquid equilibria in the system (methane + tetracosane), Fluid Phase Equilibria 127 (1997) 129–146.
[19] C.J. Peters, J.L. De Roo, J. De Swaan Arons, Three-phase equilibria in (ethane + pentacosane), The Journal of Chemical Thermodynamics 19 (1987) 265–272.
[20] N.C. Huie, K.D. Luks, J.P. Kohn, Phase-equilibriums behavior of systems carbon dioxide-n-eicosane and carbon dioxide-n-decane-n-eicosane, Journal of Chemical & Engineering Data 18 (1973) 311–313.
[21] C.J. Peters, H.J. Van Der Kooi, J. De Swaan Arons, Measurements and calculations of phase equilibria for (ethane + tetracosane) and (p, Vm^{*}, T) of liquid tetracosane, The Journal of Chemical Thermodynamics 19 (1987) 395–405.
[22] H.J. van der Kooi, E. Flöter, T.W.d. Loos, High-pressure phase equilibria of {(1-x)CH4+xCH3(CH2)18CH3}, The Journal of Chemical Thermodynamics 27 (1995) 847–861.
[23] J.J.B. Machado, T.W. de Loos, Liquid-vapour and solid-fluid equilibria for the system methane + triacontane at high temperature and high pressure, Fluid Phase Equilibria 222–223 (2004) 261–267.
[24] M.L. Corazza, L. Cardozo Filho, J. Vladmir Oliveira, C. Dariva, A robust strategy for SVL equilibrium calculations at high pressures, Fluid Phase Equilibria 221 (2004) 113–126.
[25] K. Carter, K.D. Luks, Extending a classical EOS correlation to represent solid-fluid phase equilibria, Fluid Phase Equilibria 243 (2006) 151–155.
[26] E.L. Allgower, K. Georg, in: P.G. Ciarlet, J.L. Lions (Eds.), Numerical Path Following, North-Holland, 1997.
[27] M.L. Michelsen, Calculation of phase envelopes and critical points for multicomponent mixtures, Fluid Phase Equilibria 4 (1980) 1–10.
[28] M.L. Michelsen, J.M. Mollerup, Thermodynamic Models: Fundamentals and Computational Aspects, 1st ed., Tie-Line Publications, Denmark, 2004.
[29] M. Cismondi, D.N. Nuñez, M.S. Zabaloy, E.A. Brignole, M.L. Michelsen, J.M. Mollerup, GPEC: a program for global phase equilibrium calculations in binary systems, in: EQUIFASE ĭ06-VII Iberoamerican Conference on Phase Equilibria and Fluid Properties for Process Design, Morelia, Michoacán, México, 2006.
[30] M. Cismondi, M.L. Michelsen, Global phase equilibrium calculations: critical lines, critical end points and liquid-liquid-vapour equilibrium in binary mixtures, The Journal of Supercritical Fluids 39 (2007) 287–295.
[31] M. Cismondi, M. Michelsen, Automated calculation of complete Pxy and Txy diagrams for binary systems, Fluid Phase Equilibria 259 (2007) 228–234.
[32] A. Firoozabadi, Thermodynamics of Hydrocarbon Reservoirs, 1st ed., McGraw-Hill, USA, 1999.
[33] R. Favareto, V.F. Cabral, M.L. Corazza, L. Cardozo-Filho, Vapor-liquid and solid-fluid equilibrium for progesterone + CO_2, progesterone + propane, and progesterone + n-butane systems at elevated pressures, The Journal of Supercritical Fluids 45 (2008) 161–170.
[34] D.-Y. Peng, D.B. Robinson, A new two-constant equation of state, Industrial & Engineering Chemistry Fundamentals 15 (1976) 59–64.
[35] A. Diefenbacher, M. Türk, Phase equilibria of organic solid solutes and supercritical fluids with respect to the RESS process, The Journal of Supercritical Fluids 22 (2002) 175–184.
[36] S.B. Rodriguez-Reartes, M. Cismondi, E. Franceschi, M.L. Corazza, J.V. Oliveira, M.S. Zabaloy, High-pressure phase equilibria of systems carbon dioxide + n-eicosane and propane + n-eicosane, The Journal of Supercritical Fluids 50 (2009) 193–202.
[37] DIPPR 801, Evaluated Process Design Data, Public Release in, American Institute of Chemical Engineers, Design Institute for Physical Property Data, BYU-DIPPR, Thermophysical Properties Laboratory, Provo, Utah, 2003.
[38] P. Alessi, A. Cortesi, I. Kikic, N.R. Foster, S.J. Macnaughton, I. Colombo, Particle production of steroid drugs using supercritical fluid processing, Industrial & Engineering Chemistry Research 35 (1996) 4718–4726.